Supporting Information for: Stereoselectivity in Atmospheric Autoxidation

Kristian H. Møller,[†] Eric Praske,[‡] Lu Xu,[¶] John D. Crounse,[¶] Paul O. Wennberg,[*,¶,§] and Henrik G. Kjaergaard[*,†]

[†]*Department of Chemistry, University of Copenhagen, DK-2100 Copenhagen Ø, Denmark*

[‡]*Division of Chemistry and Chemical Engineering, California Institute of Technology, Pasadena, California 91125, United States*

[¶]*Division of Geological and Planetary Sciences, California Institute of Technology, Pasadena, California 91125, United States*

[§]*Division of Engineering and Applied Science, California Institute of Technology, Pasadena, California 91125, United States*

[*]To whom correspondence should be addressed.

Contents

S1 Theoretical Methods

Reaction rate coefficients are calculated using the multi-conformer transition state theory (MC-TST) approach by Møller et al.[1] Briefly, the MC-TST reaction rate coefficient, k, is given by:[1,2]

$$k = \kappa \frac{k_B T}{h} \frac{\sum_{i}^{All\ TS\ conf.} \exp\left(\frac{-\Delta E_i}{k_B T}\right) Q_{TS_i}}{\sum_{j}^{All\ R\ conf.} \exp\left(\frac{-\Delta E_j}{k_B T}\right) Q_{R_j}} \exp\left(-\frac{E_{TS} - E_R}{k_B T}\right) \quad \text{(S1)}$$

where κ is the tunneling coefficient, k_B is Boltzmann's constant, T is the temperature, h is Planck's constant, E is the zero-point corrected energy and Q is the partition function (harmonic oscillator, rigid rotor). The final term is the difference in zero-point corrected energy between the lowest-energy conformers of transition state (TS) and reactant; the reaction barrier. The sums are formally over all transition states and reactants (R), respectively, but here, we include only those with relative electronic energies below 2 kcal/mol.[1]

The relative energy between conformers, partition functions and zero-point energy corrections are calculated using ωB97X-D/aug-cc-pVTZ in Gaussian 09, revision D.01, while the electronic energy of the lowest-energy conformers are calculated using ROCCSD(T)-F12a/VDZ-F12//ωB97X-D/aug-cc-pVTZ (abbreviated F12) in Molpro 2012.1.[3–12] This single-point correction is applied to the peroxy H-shift reactions of most of the first-generation hydroxy peroxy radicals. The exceptions are the H-shifts abstracting from -OH groups, where issues have previously been observed.[13] For these, the ωB97X-D/aug-cc-pVTZ electronic energies are used instead. The same is done for the rate coefficients in the chemical mechanism under high-NO conditions and those following the aldehydic H-shifts (Figures S16, S18 and S19).

Conformers are located using the Merck Molecular Force Field, MMFF (enforcing a neutral charge) in Spartan '14 and subsequently optimized using B3LYP/6-31+G(d) in Gaussian 09, revision D.01.[1,6,14–20] Those with electronic energies within 2 kcal/mol of the lowest-energy conformer are further optimized using ωB97X-D/aug-cc-pVTZ and included in the sums of partition functions.[1] As found in Møller et al.[1], tests indicate that conformational sampling using MMFF with a neutral charge seems to introduce only little error (see Section S2). All ωB97X-D/aug-cc-pVTZ and F12 output files, which include the ωB97X-D/aug-cc-pVTZ optimized geometries, are available at:
https://sid.erda.dk/public/archives/bfad8e9ca7cf171e6d225371b36c3372/published-archive.html

Tunneling is calculated using the Eckart approach with electronic energies at the F12 level and zero-point vibrational corrections and imaginary frequency at the

ωB97X-D/aug-cc-pVTZ level.[21] The reactant and product conformers connected to the lowest-energy transition state by an IRC are used to calculate the tunneling coefficient. Temperature dependencies of the calculated aldehydic H-shift rate coefficients are given in Table S12.

S2 Assessment of Conformational Sampling

For the reactions studied theoretically here, conformational sampling is carried out using MMFF with a neutral charge enforced, as recommended for a cost-effective approach in Møller et al.[1] To verify the validity of this approach for the reactions studied here, we calculated the rate coefficients of the 1,4 and 1,5 aldehydic H-shifts of the CRALD hydroxy peroxy radical isomers using multiple computational methods for the systematic conformational sampling. In addition to MMFF with a neutral charge (MMFF-charge), we used MMFF with the optimized atom types identified by Møller et al. (MMFF-type, with atom types 6 ("generic divalent O") and 3 ("generic carbonyl carbon") for the O- and C- centered radicals, respectively) and SYBYL.[1,22] All conformational samplings are systematic conformer searches in Spartan '14.[15]

In all four cases, no new TS conformers are identified by including the two additional computational methods in the conformational sampling, while a few additional reactant conformers are identified. As shown in Table S1, this means that the rate coefficients calculated using only MMFF-charge are slightly overestimated compared to the rate coefficients with the more involved conformational sampling. The largest effect is observed for the 3-OH,2-OO *(R,S)* with an overestimation of a little more than 25 %, primarily due to one reactant conformer with a relative energy of 0.14 kcal/mol being missed by MMFF-charge. But overall, the error introduced by using only MMFF-charge is limited.

Table S1: Calculated reaction rate coefficients including tunneling (in s^{-1}) at 298.15 K for the 1,4 and 1,5 aldehydic H-shift of the CRALD hydroxy peroxy radical. "$k_{MMFF\text{-}charge}$" uses only the conformers located by MMFF-charge, while "$k_{Combined}$" use all unique conformers located by MMFF-charge, MMFF-type and SYBYL combined. All else is as in the approach by Møller et al.

Isomer	Reaction	$k_{MMFF\text{-}charge}$	$k_{Combined}$
2-OH,3-OO *(R,R)*	1,5-C**H**O	2.9×10^{-1}	2.7×10^{-1}
2-OH,3-OO *(R,S)*	1,5-C**H**O	2.5×10^{-2}	2.2×10^{-2}
3-OH,2-OO *(R,R)*	1,4-C**H**O	2.8×10^{-1}	2.4×10^{-1}
3-OH,2-OO *(R,S)*	1,4-C**H**O	9.4×10^{-1}	7.4×10^{-1}

S3 Calculated H-shift Rate Contants and Associated Data

No F12 single-point calculations are done for the H-shifts abstracting from OH groups. For the transition states of such reactions, it has been found that the Hartree-Fock (HF) calculation providing the foundation of the F12 calculation can converge to different solutions with very different energies.[13] Instead, only the values using ωB97X-D/aug-cc-pVTZ for the barrier are calculated.

S3.1 2-Methylpropene

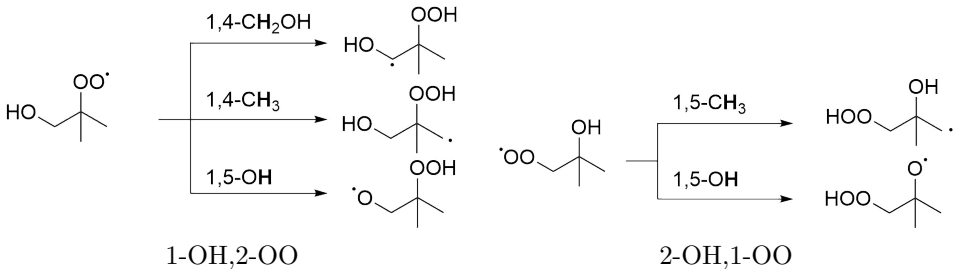

Figure S1: H-shift reactions in the two hydroxy peroxy radicals formed by OH and O_2-addition to 2-methylpropene.

Table S2: F12 calculated reaction barriers (ΔE in kcal/mol), summed ωB97X-D/aug-cc-pVTZ reactant and transition state partition functions ($\sum Q_R$ and $\sum Q_{TS}$, respectively), Eckart tunneling coefficients (κ) and MC-TST rate coefficients including tunneling (k in s^{-1}) at 298.15 K for the hydroxy peroxy radicals formed from 2-methylpropene. See Figure S1 for an illustration of the reactions. Values are calculated using the approach by Møller et al.[1]

Isomer	Reaction	ΔE	$\sum Q_R$[a]	$\sum Q_{TS}$[b]	κ	k
1-OH,2-OO	1,4-C**H**$_2$OH[c]	29.89	34177191	7200591	1.46×10^{3}	2.3×10^{-7}
1-OH,2-OO	1,4-C**H**$_3$[c]	35.69	34177191	16992349	2.68×10^{4}	5.7×10^{-10}
1-OH,2-OO	1,5-O**H**	-	-	-	-	-
2-OH,1-OO	1,5-C**H**$_3$[c]	25.14	44522934	3451932	5.15×10^{1}	9.3×10^{-6}
2-OH,1-OO	1,5-O**H**	-	-	-	-	-

[a] $\sum_{j}^{R\ conf.} \exp\left(\frac{-\Delta E_j}{k_B T}\right) Q_{R_j}$

[b] $\sum_{i}^{TS\ conf.} \exp\left(\frac{-\Delta E_i}{k_B T}\right) Q_{TS_i}$

[c] Abstraction of the hydrogen atom pointing towards the peroxy group.

Table S3: ωB97X-D/aug-cc-pVTZ calculated reaction barriers (ΔE in kcal/mol), summed reactant and transition state partition functions ($\sum Q_R$ and $\sum Q_{TS}$, respectively), Eckart tunneling coefficients (κ) and MC-TST rate coefficients including tunneling (k in s^{-1}) at 298.15 K for the hydroxy peroxy radicals formed from 2-methylpropene. See Figure S1 for an illustration of the reactions. Values are calculated using the approach by Møller et al.[1] but without the F12 single-point correction.

Isomer	Reaction	ΔE	$\sum Q_R$[a]	$\sum Q_{TS}$[b]	κ	k
1-OH,2-OO	1,4-C**H**$_2$OH[c]	30.10	34177191	7200591	8.95×10^{2}	1.0×10^{-7}
1-OH,2-OO	1,4-C**H**$_3$[c]	37.32	34177191	16992349	1.01×10^{4}	1.4×10^{-11}
1-OH,2-OO	1,5-O**H**	21.70	34177191	3936248	1.00×10^{0}	8.8×10^{-5}
2-OH,1-OO	1,5-C**H**$_3$[c]	26.06	44522934	3451932	2.68×10^{1}	1.0×10^{-6}
2-OH,1-OO	1,5-O**H**	21.25	44522934	4253735	1.54×10^{0}	2.4×10^{-4}

[a] $\sum_{j}^{R\ conf.} \exp\left(\frac{-\Delta E_j}{k_B T}\right) Q_{R_j}$

[b] $\sum_{i}^{TS\ conf.} \exp\left(\frac{-\Delta E_i}{k_B T}\right) Q_{TS_i}$

[c] Abstraction of the hydrogen atom pointing towards the peroxy group.

S3.2 Crotonaldehyde (CRALD)

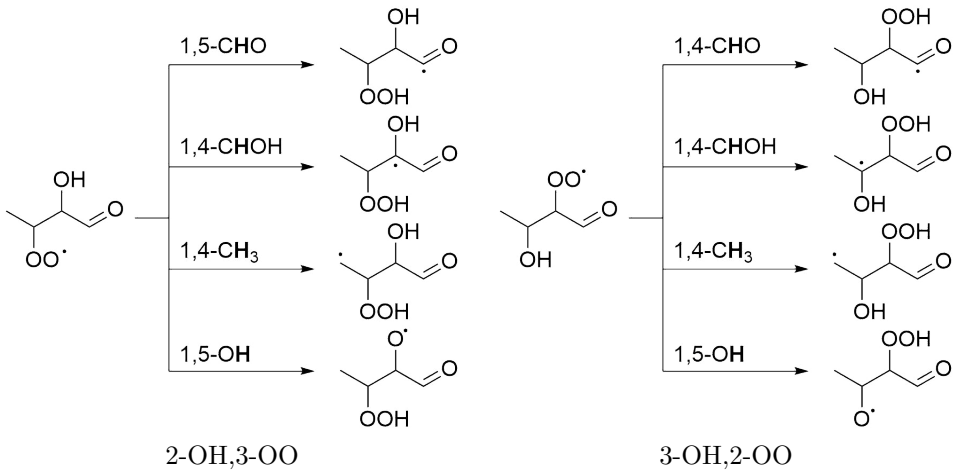

Figure S2: H-shift reactions in the two structural isomers of the hydroxy peroxy radical formed by OH and O_2-addition to crotonaldehyde.

Table S4: F12 calculated reaction barriers (ΔE in kcal/mol), summed ωB97X-D/aug-cc-pVTZ reactant and transition state partition functions ($\sum Q_R$ and $\sum Q_{TS}$, respectively), Eckart tunneling coefficients (κ) and MC-TST rate coefficients including tunneling (k in s^{-1}) at 298.15 K for the hydroxy peroxy radicals formed from crotonaldehyde. See Figure S2 for an illustration of the reactions. Values are calculated using the approach by Møller et al.[1]

Isomer	Reaction	ΔE	$\sum Q_R$[a]	$\sum Q_{TS}$[b]	κ	k
2-OH,3-OO *(R,R)*	1,5-C**H**O	20.05	265070657	21113286	2.93×10^{2}	2.9×10^{-1}
2-OH,3-OO *(R,R)*	1,4-C**H**OH	26.23	265070657	27064536	4.35×10^{5}	1.6×10^{-2}
2-OH,3-OO *(R,R)*	1,4-C**H**$_3$[c]	35.43	265070657	59969680	2.28×10^{4}	3.4×10^{-10}
2-OH,3-OO *(R,R)*	1,5-O**H**	-	-	-	-	-
2-OH,3-OO *(R,S)*	1,5-C**H**O	22.58	95708806	36564686	3.73×10^{2}	2.5×10^{-2}
2-OH,3-OO *(R,S)*	1,4-C**H**OH	25.88	95708806	16734375	3.26×10^{4}	3.8×10^{-3}
2-OH,3-OO *(R,S)*	1,4-C**H**$_3$[c]	36.51	95708806	67111481	1.55×10^{4}	1.2×10^{-10}
2-OH,3-OO *(R,S)*	1,5-O**H**	-	-	-	-	-
3-OH,2-OO *(R,R)*	1,4-C**H**O	20.64	123730250	44022245	1.69×10^{2}	2.8×10^{-1}
3-OH,2-OO *(R,R)*	1,4-C**H**OH	24.23	123730250	14803444	1.47×10^{2}	1.9×10^{-4}
3-OH,2-OO *(R,R)*	1,5-C**H**$_3$[c]	24.88	123730250	21193015	3.98×10^{1}	2.5×10^{-5}
3-OH,2-OO *(R,R)*	1,5-O**H**	-	-	-	-	-
3-OH,2-OO *(R,S)*	1,4-C**H**O	19.75	375546871	85340376	1.98×10^{2}	9.4×10^{-1}
3-OH,2-OO *(R,S)*	1,4-C**H**OH	25.74	375546871	45657235	4.91×10^{2}	5.1×10^{-5}
3-OH,2-OO *(R,S)*	1,5-C**H**$_3$[c]	25.26	375546871	39824255	5.83×10^{1}	1.2×10^{-5}
3-OH,2-OO *(R,S)*	1,5-O**H**	-	-	-	-	-

[a] $\sum_{j}^{R\ conf.} \exp\left(\frac{-\Delta E_j}{k_B T}\right) Q_{R_j}$

[b] $\sum_{i}^{TS\ conf.} \exp\left(\frac{-\Delta E_i}{k_B T}\right) Q_{TS_i}$

[c] Abstraction of the hydrogen atom pointing towards the peroxy group.

Table S5: ωB97X-D/aug-cc-pVTZ calculated reaction barriers (ΔE in kcal/mol), summed reactant and transition state partition functions ($\sum Q_R$ and $\sum Q_{TS}$, respectively), Eckart tunneling coefficients (κ) and MC-TST rate coefficients including tunneling (k in s^{-1}) at 298.15 K for the hydroxy peroxy radicals formed from crotonaldehyde. See Figure S2 for an illustration of the reactions. Values are calculated using the approach by Møller et al.[1] but without the F12 single-point correction.

Isomer	Reaction	ΔE	$\sum Q_R$[a]	$\sum Q_{TS}$[b]	κ	k
2-OH,3-OO *(R,R)*	1,5-C**H**O	19.58	265070657	21113286	1.35×10^{2}	3.0×10^{-1}
2-OH,3-OO *(R,R)*	1,4-C**H**OH	24.48	265070657	27064536	2.17×10^{5}	1.6×10^{-1}
2-OH,3-OO *(R,R)*	1,4-C**H**$_3$[c]	37.52	265070657	59969680	1.12×10^{4}	4.9×10^{-12}
2-OH,3-OO *(R,R)*	1,5-O**H**	21.26	265070657	25875168	1.72×10^{0}	2.7×10^{-4}
2-OH,3-OO *(R,S)*	1,5-C**H**O	21.73	95708806	36564686	1.68×10^{2}	4.7×10^{-2}
2-OH,3-OO *(R,S)*	1,4-C**H**OH	24.35	95708806	16734375	2.20×10^{4}	3.4×10^{-2}
2-OH,3-OO *(R,S)*	1,4-C**H**$_3$[c]	38.15	95708806	67111481	8.30×10^{3}	4.0×10^{-12}
2-OH,3-OO *(R,S)*	1,5-O**H**	20.95	95708806	25391847	1.00×10^{0}	7.2×10^{-4}
3-OH,2-OO *(R,R)*	1,4-C**H**O	21.14	123730250	44022245	1.31×10^{2}	9.2×10^{-2}
3-OH,2-OO *(R,R)*	1,4-C**H**OH	24.27	123730250	14803444	1.29×10^{2}	1.6×10^{-4}
3-OH,2-OO *(R,R)*	1,5-C**H**$_3$[c]	25.41	123730250	21193015	2.19×10^{1}	5.5×10^{-6}
3-OH,2-OO *(R,R)*	1,5-O**H**	22.03	123730250	29365073	1.78×10^{0}	1.9×10^{-4}
3-OH,2-OO *(R,S)*	1,4-C**H**O	20.62	375546871	85340376	1.61×10^{2}	1.8×10^{-1}
3-OH,2-OO *(R,S)*	1,4-C**H**OH	25.83	375546871	45657235	3.71×10^{2}	3.3×10^{-5}
3-OH,2-OO *(R,S)*	1,5-C**H**$_3$[c]	26.02	375546871	39824255	3.09×10^{1}	1.7×10^{-6}
3-OH,2-OO *(R,S)*	1,5-O**H**	20.01	375546871	24168507	1.00×10^{0}	8.6×10^{-4}

[a] $\sum_{j}^{R\ conf.} \exp\left(\frac{-\Delta E_j}{k_B T}\right) Q_{R_j}$

[b] $\sum_{i}^{TS\ conf.} \exp\left(\frac{-\Delta E_i}{k_B T}\right) Q_{TS_i}$

[c] Abstraction of the hydrogen atom pointing towards the peroxy group.

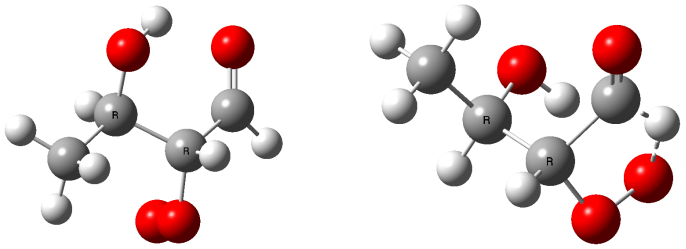

Reactant *(R,R)* TS *(R,R)*

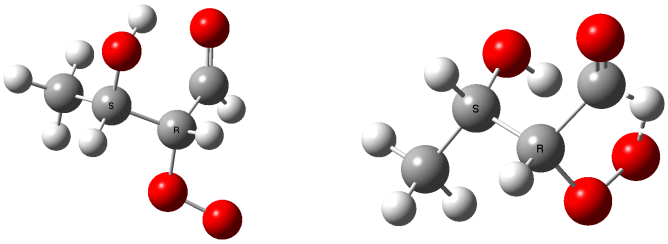

Reactant *(R,S)* TS *(R,S)*

Figure S3: Structures of the lowest-energy (ωB97X-D/aug-cc-pVTZ) reactant and TS conformers of 3-OH,2-OO-CRALD

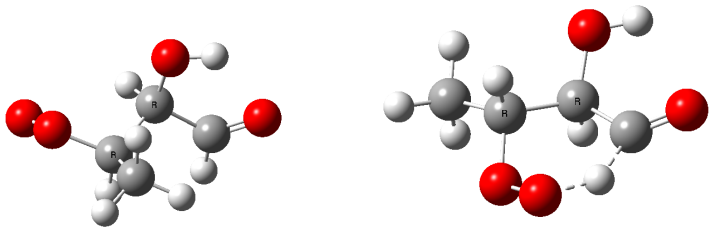

Reactant *(R,R)* TS *(R,R)*

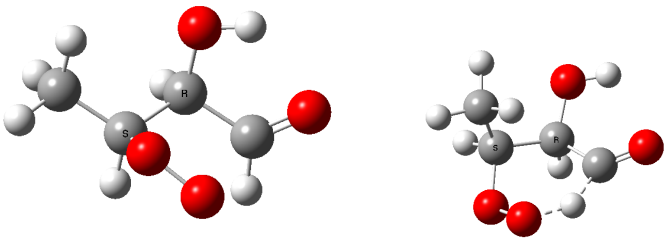

Reactant *(R,S)* TS *(R,S)*

Figure S4: Structures of the lowest-energy (ωB97X-D/aug-cc-pVTZ) reactant and TS conformers of 2-OH,3-OO-CRALD

Isomer	Reactant	TS	Barrier (TS-Reactant)
2-OH-3-OO	0.88	-1.64	-2.53
3-OH-2-OO	-1.32	-0.43	0.90

Table S6: Energy difference (in kcal/mol) between the *(R,R)* and *(R,S)* diastereomers (i.e. *(R,R)-(R,S)*) for the reactant, TS and barrier height in the two stereoisomers in crotonaldehyde oxidation. Electronic energies are calculated using CCSD(T)-F12a/VDZ-F12//ωB97X-D/aug-cc-pVTZ and zero-point vibrational corrections are calculated using ωB97X-D/aug-cc-pVTZ.

S3.3 Acrolein (ACR)

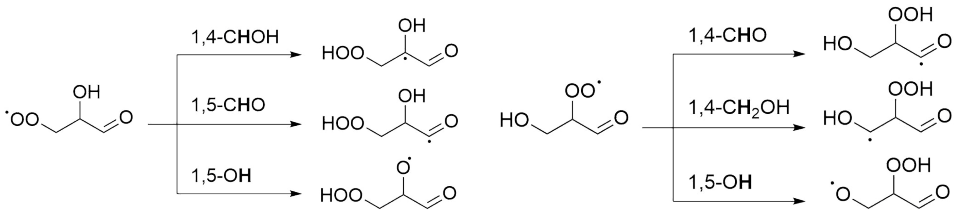

Figure S5: H-shift reactions in the two hydroxy peroxy radicals formed by OH and O_2-addition to acrolein.

Table S7: F12 calculated reaction barriers (ΔE in kcal/mol), summed ωB97X-D/aug-cc-pVTZ reactant and transition state partition functions ($\sum Q_R$ and $\sum Q_{TS}$, respectively), Eckart tunneling coefficients (κ) and MC-TST rate coefficients including tunneling (k in s^{-1}) at 298.15 K for the hydroxy peroxy radicals formed from acrolein. See Figure S5 for an illustration of the reactions. Values are calculated using the approach by Møller et al.[1]

Isomer	Reaction	ΔE	$\sum Q_R$[a]	$\sum Q_{TS}$[b]	κ	k
2-OH,3-OO	1,4-C**H**OH	26.44	32964458	4853872	3.98×10^{4}	1.5×10^{-3}
2-OH,3-OO	1,5-C**H**O	21.82	32964458	5167411	3.65×10^{2}	3.6×10^{-2}
2-OH,3-OO	1,5-O**H**	-	-	-	-	-
3-OH,2-OO	1,4-C**H**O	21.35	114841459	16655717	2.43×10^{2}	4.9×10^{-2}
3-OH,2-OO	1,4-C**H**$_2$OH[c]	28.66	114841459	8791438	1.44×10^{3}	6.7×10^{-7}
3-OH,2-OO	1,5-O**H**	-	-	-	-	-

[a] $\sum_{j}^{R\ conf.} \exp\left(\frac{-\Delta E_j}{k_B T}\right) Q_{R_j}$

[b] $\sum_{i}^{TS\ conf.} \exp\left(\frac{-\Delta E_i}{k_B T}\right) Q_{TS_i}$

[c] Abstraction of the hydrogen atom pointing towards the peroxy group.

Table S8: ωB97X-D/aug-cc-pVTZ calculated reaction barriers (ΔE in kcal/mol), summed reactant and transition state partition functions ($\sum Q_R$ and $\sum Q_{TS}$, respectively), Eckart tunneling coefficients (κ) and MC-TST rate coefficients including tunneling (k in s^{-1}) at 298.15 K for the hydroxy peroxy radicals formed from acrolein. See Figure S5 for an illustration of the reactions. Values are calculated using the approach by Møller et al.[1] but without the F12 single-point correction.

Isomer	Reaction	ΔE	$\sum Q_R$[a]	$\sum Q_{TS}$[b]	κ	k
2-OH,3-OO	1,4-C**H**OH	25.13	32964458	4853872	2.65×10^{4}	9.2×10^{-3}
2-OH,3-OO	1,5-C**H**O	20.88	32964458	5167411	1.71×10^{2}	8.2×10^{-2}
2-OH,3-OO	1,5-O**H**	22.09	32964458	8555317	1.52×10^{0}	1.6×10^{-4}
3-OH,2-OO	1,4-C**H**O	21.25	114841459	16655717	1.76×10^{2}	4.2×10^{-2}
3-OH,2-OO	1,4-C**H**$_2$OH[c]	28.76	114841459	8791438	1.03×10^{3}	4.1×10^{-7}
3-OH,2-OO	1,5-O**H**	21.16	114841459	4673593	1.00×10^{0}	7.9×10^{-5}

[a] $\sum_{j}^{R\ conf.} \exp\left(\frac{-\Delta E_j}{k_B T}\right) Q_{R_j}$

[b] $\sum_{i}^{TS\ conf.} \exp\left(\frac{-\Delta E_i}{k_B T}\right) Q_{TS_i}$

[c] Abstraction of the hydrogen atom pointing towards the peroxy group.

S3.4 Methacrolein (MACR)

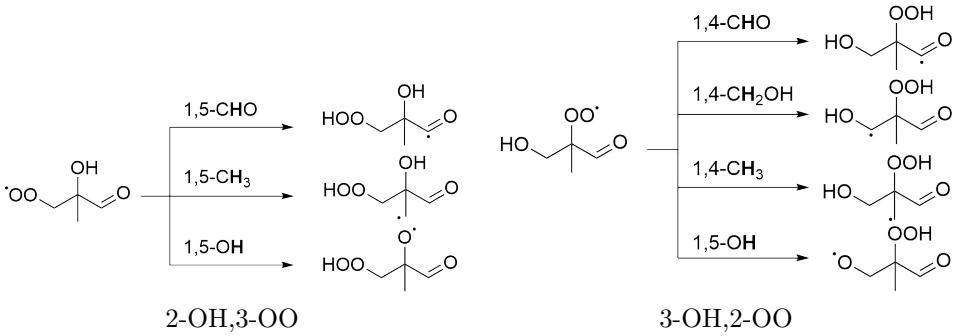

Figure S6: H-shift reactions in the two hydroxy peroxy radicals formed by OH and O_2-addition to methacrolein.

Table S9: F12 calculated reaction barriers (ΔE in kcal/mol), summed ωB97X-D/aug-cc-pVTZ reactant and transition state partition functions ($\sum Q_R$ and $\sum Q_{TS}$, respectively), Eckart tunneling coefficients (κ) and MC-TST rate coefficients including tunneling (k in s^{-1}) at 298.15 K for the hydroxy peroxy radicals formed from methacrolein. See Figure S6 for an illustration of the reactions. Values are calculated using the approach by Møller et al. [1]

Isomer	Reaction	ΔE	$\sum Q_R$[a]	$\sum Q_{TS}$[b]	κ	k
2-OH,3-OO	1,5-C**H**O	20.97	166400098	31604437	9.90×10^{1}	5.0×10^{-2}
2-OH-3-OO	1,5-C**H**$_3$[c]	26.42	166400098	38821769	4.92×10^{1}	3.0×10^{-6}
2-OH-3-OO	1,5-O**H**	-	-	-	-	-
3-OH,2-OO	1,4-C**H**O	20.26	162721827	50730621	1.51×10^{2}	4.2×10^{-1}
3-OH,2-OO	1,4-C**H**$_2$OH[c]	25.50	162721827	13006276	2.93×10^{2}	3.0×10^{-5}
3-OH,2-OO	1,4-C**H**$_3$[c]	35.68	162721827	61206759	9.34×10^{3}	1.5×10^{-10}
3-OH,2-OO	1,5-O**H**	-	-	-	-	-

[a] $\sum_{j}^{R\ conf.} \exp\left(\frac{-\Delta E_j}{k_B T}\right) Q_{R_j}$

[b] $\sum_{i}^{TS\ conf.} \exp\left(\frac{-\Delta E_i}{k_B T}\right) Q_{TS_i}$

[c] Abstraction of the hydrogen atom pointing towards the peroxy group.

Table S10: ωB97X-D/aug-cc-pVTZ calculated reaction barriers (ΔE in kcal/mol), summed reactant and transition state partition functions ($\sum Q_R$ and $\sum Q_{TS}$, respectively), Eckart tunneling coefficients (κ) and MC-TST rate coefficients including tunneling (k in s^{-1}) at 298.15 K for the hydroxy peroxy radicals formed from methacrolein. See Figure S6 for an illustration of the reactions. Values are calculated using the approach by Møller et al.[1] but without the F12 single-point correction.

Isomer	Reaction	ΔE	$\sum Q_R$[a]	$\sum Q_{TS}$[b]	κ	k
2-OH,3-OO	1,5-C**H**O	20.01	166400098	31604437	6.25×10^{1}	1.6×10^{-1}
2-OH-3-OO	1,5-C**H**$_3$[c]	27.09	166400098	38821769	2.80×10^{1}	5.6×10^{-7}
2-OH-3-OO	1,5-O**H**	21.33	166400098	35707816	1.07×10^{0}	3.3×10^{-4}
3-OH,2-OO	1,4-C**H**O	20.63	162721827	50730621	1.18×10^{2}	1.7×10^{-1}
3-OH,2-OO	1,4-C**H**$_2$OH[c]	25.62	162721827	13006276	2.20×10^{2}	1.8×10^{-5}
3-OH,2-OO	1,4-C**H**$_3$[c]	37.05	162721827	61206759	4.45×10^{3}	7.3×10^{-12}
3-OH,2-OO	1,5-O**H**	20.69	162721827	17079193	1.00×10^{0}	4.5×10^{-4}

[a] $\sum_{j}^{R\ conf.} \exp\left(\frac{-\Delta E_j}{k_B T}\right) Q_{R_j}$

[b] $\sum_{i}^{TS\ conf.} \exp\left(\frac{-\Delta E_i}{k_B T}\right) Q_{TS_i}$

[c] Abstraction of the hydrogen atom pointing towards the peroxy group.

S4 Comparison of Aldehydic H-shifts in Crotonaldehyde, Methacrolein and Acrolein

The structure of crotonaldehyde is similar to those of acrolein and methacrolein (see Figure S7), which are both important molecules in the atmosphere.[23–25] As for crotonaldehyde, these can react with OH by addition at either the 2- or 3-position followed by O_2-addition leading to two different hydroxy peroxy radicals. Table S11 compares the calculated rate coefficients (at 298.15 K, which is slightly warmer than the present experiments) of the 1,4 and 1,5 aldehydic H-shifts in the hydroxy peroxy radicals of acrolein, methacrolein and crotonaldehyde. All eight calculated rate coefficients are similar and fall within the range of 0.01 s^{-1} - 1 s^{-1}, in good agreement with the range reported in the previous study on isoprene oxidation.[13] In most cases, the 1,4 H-shift is calculated to be faster than the corresponding 1,5 H-shift, which is surprising, as for non-aldehydic H-shifts, 1,4 H-shifts are typically much slower than their 1,5 H-shift counterparts.[26] As with crotonaldehyde, the non-aldehydic H-shifts in the hydroxy peroxy radicals of acrolein and methacrolein are calculated to be much slower and of no importance in the atmosphere (see Tables S8-S9).

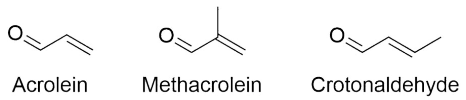

Figure S7: Structures of acrolein, methacrolein and crotonaldehyde

Table S11: Calculated[a] rate coefficients (s^{-1}) at 298.15 K[b] for the 1,4 and 1,5 aldehydic H-shifts in the hydroxy peroxy radicals formed by OH and O_2-addition to the different precursors.

System	1,4 H-shift	1,5 H-shift
Acrolein	4.9×10^{-2}	3.6×10^{-2}
Methacrolein	4.2×10^{-1}[c]	3.5×10^{-2}
Crotonaldehyde *(R,R)*[d]	2.8×10^{-1}	2.9×10^{-1}
Crotonaldehyde *(R,S)*[d]	9.4×10^{-1}	2.5×10^{-2}

[a] Calculated using the approach by Møller et al.[1]

[b] Note that the temperature here is slightly higher than in Table 1 in the main manuscript.

[c] This value differs slightly from the one previously published using the same approach.[1] The main difference stems from the inclusion here of a reactant conformer which is an IRC end-point from one of the other H-shifts of the peroxy radical.

[d] Crotonaldehyde itself is achiral, but the hydroxy peroxy radicals formed have two chiral centers.

S5 Temperature Dependence of Calculated Aldehydic H-shift Rate Coefficients

The temperature dependence of the rate coefficients, k, is fitted as:[27–29]

$$k = Ae^{-B/T}e^{C/T^3} \tag{S2}$$

The temperature dependent rate coefficients are determined from independent fits to rate coefficients (without tunneling) and tunneling coefficients calculated in the temperature range from 290 K - 320 K in steps of 5 K. B is obtained from the fit of the rate coefficients and C from the fit of the tunneling coefficients, while A is the product of the prefactors from the two independent fits. These fits reproduce the calculated rate coefficients for all reactions and temperatures to within 0.5 %.

Table S12: A (s^{-1}), B (K) and C (K^3) parameters used to reproduce calculated temperature dependent reaction rate coefficients.

Isomer	Reaction	A	B	C
CRALD-2-OH,3-OO *(R,R)*	1,5-C**H**O	6.53×10^{11}	1.00×10^{4}	1.35×10^{8}
CRALD-2-OH,3-OO *(R,S)*	1,5-C**H**O	4.59×10^{12}	1.14×10^{4}	1.40×10^{8}
CRALD-3-OH,2-OO *(R,R)*	1,4-C**H**O	4.22×10^{12}	1.05×10^{4}	1.31×10^{8}
CRALD-3-OH,2-OO *(R,S)*	1,4-C**H**O	1.89×10^{12}	9.96×10^{3}	1.35×10^{8}
ACR-2-OH,3-OO	1,5-C**H**O	7.70×10^{11}	1.08×10^{4}	1.43×10^{8}
ACR-3-OH,2-OO	1,4-C**H**O	9.58×10^{11}	1.07×10^{4}	1.43×10^{8}
MACR-2-OH,3-OO	1,5-C**H**O	6.59×10^{11}	1.03×10^{4}	1.17×10^{8}
MACR-3-OH,2-OO	1,4-C**H**O	2.60×10^{12}	1.02×10^{4}	1.27×10^{8}

S6 Alkyl Radical Stability

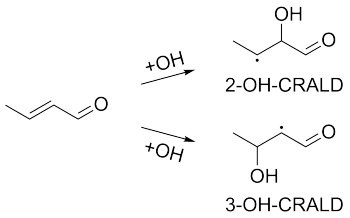

Figure S8: The two alkyl radical structural isomers formed by OH-addition to crotonaldehyde.

Isomer	Rel. E
2-OH-CRALD	6.94
3-OH-CRALD	0.0

Table S13: Relative energy (electronic energy + zero-point vibrational correction, in kcal/mol) of the lowest-energy conformer of the two alkyl radical structural isomers formed by OH-addition to crotonaldehyde. The electronic energy is calculated at the F12 level, while the zero-point vibrational correction is at the ωB97X-D/aug-cc-pVTZ level.

S7 Comparison of Alkoxy Bond Scissions

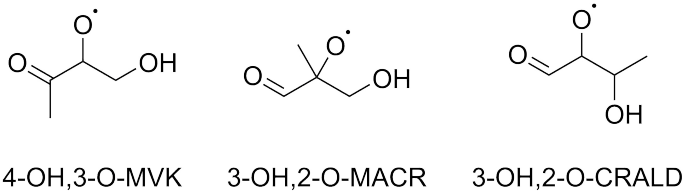

Figure S9: Structures of the alkoxy radicals whose bond scission reaction barriers are given in Table S14. The peroxy radicals are derived from methyl vinyl ketone (MVK), methacrolein (MACR) and crotonaldehyde (CRALD) by addition of OH and O_2 and reaction with NO.

Isomer	Carbonyl	Hydroxy	Methyl
4-OH,3-OO-MVK	2.4	6.1	-
3-OH,2-O-MACR	3.1	5.6	15.2
3-OH,2-O-CRALD *(R,R)*	5.3	2.2	-
3-OH,2-O-CRALD *(R,S)*	5.0	2.9	-

Table S14: ωB97XD/aug-cc-pVTZ barrier heights (kcal/mol) for alkoxy bond scission in the direction of the specified substituent.

S8 Determination of CIMS Sensitivities

CIMS sensitivities of the various products are determined based on a measured sensitivity towards glycolaldehyde and collision rate coefficients with CF_3O^- determined using the empirical approach by Su et al.[30] Dipole moments and polarizabilities of species entering into the empirical expression are calculated using the approach described earlier:[31–33] Conformers are located using a systematic conformer search with MMFF in Spartan '14 or '16.[15,34] The resulting structures are optimized using B3LYP/6-31+G(d) in Gaussian 09, rev. D.01. Structures with electronic energies no more than 15 kJ/mol above the lowest-energy structure are further optimized using B3LYP/cc-pVTZ. This level has shown good agreement with the higher B3LYP/aug-cc-pVTZ level.[35] The average dipole moment is calculated as a Boltzmann weighted

average at 298 K based on electronic energies, while the polarizability of the lowest-energy conformer is used.[35] Based on the calculated collision rate coefficients with CF_3O^- (k_x), the CIMS sensitivity of a compound (c_x) is calculated using the corresponding values for glycolaldehyde by:

$$c_x = \frac{k_x}{k_{glycolaldehyde}} \times c_{glycolaldehyde} \tag{S3}$$

Glycolaldehyde has a calculated collision rate coefficient with CF_3O^- of 2.06×10^{-9} cm^3 molecule^{-1} s^{-1} and a measured CIMS sensitivity of 1.50×10^{-4} ncts pptv^{-1}.[35] The sensitivities determined using this approach are given in Table S15.

For H_2O_2, which is used to determine the concentration of HO_2 for the bimolecular lifetime, a measured sensitivity of 7.2×10^{-5} ncts pptv^{-1} is used. This value is determined here using a calibration: The H_2O_2 concentration in a solution is determined using an UV absorption cross-section in water of 43.6 M^{-1} cm^{-1} at 240 nm.[36] A known mass of this solution is evaporated into the chamber, the CIMS signal is measured and thus the sensitivity can be determined.

Table S15: Boltzmann averaged dipole moment (μ in D), polarizability of lowest-energy conformer (α in Å^3), molecular mass (m in amu), calculated collision rate coefficient with CF_3O^- (k in cm^3 molecule^{-1} s^{-1}) and CIMS sensitivity (c in ncts pptv^{-1}) for the hydroxy nitrates and hydroxy hydroperoxides.

	μ	α	m	k	c
Glycolaldehyde	2.33	4.64	60	2.06×10^{-9}	1.50×10^{-4}[a]
2-OH,3-OOH-CRALD *(R,R)*	2.47	9.58	120	2.00×10^{-9}	1.46×10^{-4}
2-OH,3-OOH-CRALD *(R,S)*	2.27	9.59	120	1.88×10^{-9}	1.37×10^{-4}
2-OH,3-ONO_2-CRALD *(R,R)*	2.03	11.06	149	1.73×10^{-9}	1.26×10^{-4}
2-OH,3-ONO_2-CRALD *(R,S)*	1.81	11.02	149	1.62×10^{-9}	1.17×10^{-4}
3-OH,2-OOH-CRALD *(R,R)*	2.53	9.33	120	2.03×10^{-9}	1.47×10^{-4}
3-OH,2-OOH-CRALD *(R,S)*	2.35	9.34	120	1.93×10^{-9}	1.40×10^{-4}
3-OH,2-ONO_2-CRALD *(R,R)*	1.29	11.11	149	1.39×10^{-9}	1.01×10^{-4}
3-OH,2-ONO_2-CRALD *(R,S)*	2.22	11.07	149	1.83×10^{-9}	1.33×10^{-4}
1-OH,2-OOH,2-Me-propene	2.38	9.35	106	2.00×10^{-9}	1.45×10^{-4}
1-OH,2-ONO_2,2-Me-propene	2.71	10.87	135	2.13×10^{-9}	1.55×10^{-4}
2-OH,1-OOH,2-Me-propene	2.91	9.38	106	2.30×10^{-9}	1.67×10^{-4}
2-OH,1-ONO_2,2-Me-propene	2.80	11.02	135	2.18×10^{-9}	1.59×10^{-4}

[a] Experimental value.[35]

S9 Experimental Methods

The reaction rate coefficients of the peroxy radical H-shifts are determined by monitoring their competition with the bimolecular reactions with NO and HO_2. Specifically, we monitor the decreasing formation of crotonaldehyde hydroxy nitrates as a function of increasing bimolecular lifetime that results from decreasing the amounts of NO and HO_2, an approach employed previously for other compounds.[29,35,37,38] Based on known or parametrized values for the bimolecular rate coefficients, the unimolecular rate coefficients are inferred. 2-methylpropene is oxidized alongside crotonaldehyde serving as a reference whose unimolecular H-shift reactions are calculated to be much too slow to matter under the experimental conditions employed (see Section S3.1). The reference compound is used to account for variation in the concentrations of OH and NO between experiments. In the absence of unimolecular chemistry, the ratio of the yields of 2-methylpropene and crotonaldehyde hydroxy nitrates should remain constant between experiments in the limit where all peroxy radicals react with NO. Changes in the ratios are interpreted as arising from unimolecular chemistry.

Experiments are performed in a ~1 m^3 chamber consisting of a flourinated ethylene propylene copolymer (Teflon FEP, DuPont) bag at ambient atmospheric pressure (~745 Torr) and temperature (296 K). A standard mixture of 10:1 crotonaldehyde (2-butenal, ≥99% Sigma-Aldrich, predominantly trans) and 2-methylpropene (99 %, Sigma-Aldrich) is prepared in a 3 L glass bulb and diluted with N_2. The ratio is confirmed using FT-IR (Nicolet Magna-IR 560) with cross sections from the PNNL (Pacific Northwest National Laboratory) database.[39] The stability of the mixture is confirmed by regular experiments with high NO mixing ratios. The desired amount of this mixture is added to the chamber by filling an evacuated 500 cm^3 glass bulb to the desired pressure and filling this with N_2 to ambient pressure. Dry zero-air is flown through the bulb and into the chamber using an MKS flow controller at 20 standard liters per minute. For experiments with added NO, an evacuated 500 cm^3 glass bulb is filled to the desired pressure of NO (1993 ± 20 ppm in N_2, Matheson) and diluted with N_2 to slightly above atmospheric pressure. Again, zero air is flushed through the bulb to transfer its contents to the chamber. The initial chamber NO mixing ratio is measured using a chemiluminescence NO_x monitor (Teledyne NOx M200EU).

Photolysis of methylnitrite (CH_3ONO) is used as a source of OH, NO and HO_2 following the schemes below:[37,40]

$$CH_3ONO + h\nu + O_2 \rightarrow HO_2 + NO + HCHO$$

$$HO_2 + NO \rightarrow OH + NO_2$$

The methyl nitrite is synthesized and purified using an approach similar to that by Taylor et al. and stored under liquid N_2.[41] The desired amount is prepared by serial

dilution with N_2 in a 500 cm^3 glass bulb and added to the chamber as described above. Due to interferences from CH_3ONO in the NO_x monitor, the initial NO mixing ratios are measured before addition of methyl nitrite. Typical initial chamber concentrations are 100 ppb CRALD, 10 ppb 2-methylpropene, 0-1.2 ppm NO and 90 ppb CH_3ONO. The experimental details of all experiments are given in Table S16.

Photoxidation is initiated by turning on the lights (Sylvania F40/350BL, $\lambda_{max} \sim 350$ nm), initiating the CH_3ONO photolysis. Oxidation is allowed to continue for between 10 min and 17 hours depending on the experimental conditions.

Products are measured using chemical ionization time-of-flight mass spectrometry (CI-ToF-MS, Tofwerk, Caltech) with a 10 Hz temporal resolution, as described in detail before.[42,43] The CIMS reagent ion CF_3O^- is produced by flowing CF_3OOCF_3 (1 ppm in N_2) through a radioactive ^{210}Po source. Products are identified as adducts with CF_3O^- (m/z 85). The CF_3O^- ions interact with the analytes at a pressure of 26 Torr (35 mbar). All CIMS signals are normalized to the sum of $^{13}CF_3O^-$ (m/z 86) and its water adduct $^{13}CF_3O^- \cdot H_2O$ (m/z 104). CIMS sensitivities of the various products are estimated using the empirical approach of Su et al. with dipole moments and polarizabilities of species calculated using the approach described earlier and outlined in Section S8.[30–33]

The stereoisomeric compounds, including the hydroxy nitrates of interest, are separated using a gas chromatography column placed in a Varian CP-3800 gas chromatograph (GC) oven. Flow from the chamber is cryotrapped (-35 °C) for 20 minutes at the head of an 11.5 m Restek RTX-200 megabore GC column (I.D. = 0.53 mm, d_f = 3.00 μm) in an isopropanol/ethanol bath cooled to about 235 K using liquid nitrogen. No valves or metal fittings are used. The following GC temperature profile is used for the separation: Start 30 °C, 10 °C min^{-1} from 30 °C to 60 °C, hold 32 min, 20 °C min^{-1} from 60 °C to 120 °C, hold 1.5 min. This means that all the species of interest for the chemical analysis elute at the same temperature (60 ° C). A column flow of 5 sccm N_2 is used for elution. Three consecutive gas chromatograms are recorded for each experiment and their results are later averaged. Peak areas are obtained from the GCs using "peakfit" in MATLAB R2016B.[44,45] Background GCs are recorded before oxidation and any signal present in these are fitted and subtracted from the post-oxidation signals. All peaks are fitted using an exponentially-broadened Gaussian peak shape (a Gaussian peak convoluted with an exponential decay).[44] For each peak in the chromatogram, the optimal width and exponential-decay parameter is determined for a high-NO experiment and these values are used throughout all experiments.

Experiments are conducted with different concentrations of HO_2 and NO to vary the bimolecular lifetime of the peroxy radical ($\tau_{bimolecular}$), as given by:

$$\tau_{bimolecular} = \frac{1}{k_{RO_2+NO}[NO] + k_{RO_2+HO_2}[HO_2]} \quad \text{(S4)}$$

Under the conditions of the experiments, RO_2+RO_2 chemistry is calculated to be negligible based on inferred RO_2 mixing ratios and an estimated rate coefficient of 1.3 $\times 10^{-12}$ cm^3 molecule^{-1} s^{-1} based on the experimental rate coefficient for $CH_3C(O)CH_2O_2$ + $CH_3C(O)CH_2O_2$ (see Section S12).[46] For the high-NO experiments, characterized by observable no formation of H_2O_2 and hydroxy hydroperoxides (ROOH), the bimolecular lifetime is determined from the measured initial NO concentrations and assuming a standard bimolecular rate coefficient for the crotonaldehyde hydroxy peroxy radicals with NO of 8.8×10^{-12} cm^3 molecule^{-1} s^{-1} at 296 K.[28] In the experiments with little to no NO added, the bimolecular lifetime is estimated based on inferred NO and HO_2 mixing ratios and bimolecular rate coefficients, following the procedure outlined in the literature and Section S11.[29,33,38] For RO_2+HO_2, we assume a rate coefficient of 1.7×10^{-11} cm^3 molecule^{-1} s^{-1} at 296 K, as estimated using the parametrization by Wennberg et al.[28]

For each experiment, the area of each crotonaldehyde-derived HN peak is normalized to the area of 2-methyl-1-hydroxy-2-nitrooxypropene (the second 2-methylpropene-derived hydroxy nitrate peak in the chromatograms) to account for inter-experimental variation in exposure to OH and NO. Only this isomer is used, as we find that the 2-methyl-2-hydroxy-1-nitrooxypropene isomer (first GC peak) is also formed from reaction with NO_3 (see Section S18). Dividing the peak areas of the crotonaldehyde HNs with the peak area of the second 2-methylpropene hydroxy nitrate peak allows us to normalize across the different experiments and assess the unimolecular chemistry of the crotonaldehyde hydroxy peroxy radicals. This ratio will be referred to as the normalized crotonaldehyde hydroxy nitrate yield. The H-shift rate coefficients are extracted by fitting a simple chemical model (Section S13) to the normalized crontonaldehyde HN yield as a function of the determined bimolecular lifetime. The H-shift rate coefficient represents the fitting variable and is obtained from weighted least squares fit to the data. The uncertainty in the experimental values is determined from Monte Carlo analysis of the experimental data with estimated uncertainties in the bimolecular lifetime and peak area ratio. A full description is given in Section S14.

Earlier studies using a similar approach to determine the rate coefficients of unimolecular H-shift reactions have used isomers of the compound of interest whose unimolecular chemistry is calculated to be slow as internal references.[29,35,38] The approach used here employs an external reference compound (2-methylpropene) and is thus slightly more general, as it can be used in cases where all isomers have rapid unimolecular chemistry, as is the case here. The disadvantage of the use of an external reference is a slightly larger uncertainty e.g. due to potential variations in the ratio of the two species in the mixture or in the relative rates of their bimolecular chemistry with NO or HO_2. However, as the same mixture is used for all experiments,

the former is likely limited.

S10 Initial Mixing Ratios

Table S16: Initial chamber mixing ratios (ppb) in the different experiments. The NO mixing ratio is based on the NO_x monitor measurements, while the remaining values are based on the pressures measured during chamber preparation. 0.0 indicates no NO added.

Expt.	CRALD	2-Me-prop	CH_3ONO	NO
A	100.3	10.0	267.9	0.0
B	110.8	11.1	99.1	12.2
C	114.6	11.5	87.5	457.3
D	104.3	10.4	87.4	0.0
E	100.6	10.1	86.4	526.9
F	105.3	10.5	86.7	0.0
G	106.7	10.7	85.9	0.0
H	101.4	10.1	88.9	1222.7
I	100.3	10.0	75.8	7.8
J	104.4	10.4	77.5	531.0
K	70.9	7.1	105.4	0.0
L	68.7	6.9	86.7	0.0
M	72.4	7.2	93.1	0.0
N	147.5	14.8	100.7	581.0

S11 Determination of Bimolecular Lifetime

Experiments are conducted with different concentrations of NO and HO_2 to vary the bimolecular lifetime ($\tau_{bimolecular}$) of the crotonaldehyde peroxy radical, as given by:

$$\tau_{bimolecular} = \frac{1}{k_{RO_2+NO}[NO] + k_{RO_2+HO_2}[HO_2]} \tag{S5}$$

The bimolecular rate coefficients for the reaction of the crotonaldehyde hydroxy peroxy radicals with NO and HO_2 are assumed to be isomer independent and determined using the recently updated parametrizations:[28]

$$k_{RO_2+NO} = \left(2.7 \times 10^{-12}\right) \mathrm{e}^{(350\mathrm{K}/T)} \mathrm{cm}^3\ \mathrm{molecule}^{-1}\ \mathrm{s}^{-1} \tag{S6}$$

$$k_{RO_2+HO_2} = \left(2.82 \times 10^{-13}\right) \mathrm{e}^{(1300\mathrm{K}/T)} \left[1 - \mathrm{e}^{(-0.231n)}\right] \mathrm{cm}^3\ \mathrm{molecule}^{-1}\ \mathrm{s}^{-1}, \tag{S7}$$

where n = C + O + N - 2, i.e. the sum of all non-hydrogen atoms apart from the peroxy group. For the crotonaldehyde hydroxy peroxy radicals at 296 K, this

evaluates to $k_{RO_2+NO} = 8.8 \times 10^{-12}$ cm^3 molecule^{-1} s^{-1} and $k_{RO_2+HO_2} = 1.7 \times 10^{-11}$ cm^3 molecule^{-1} s^{-1}.

For the experiments with high initial NO mixing ratios and no observed growth of hydroperoxides, the bimolecular lifetime is determined from the initial NO mixing ratios as measured by the chemiluminescence NOx monitor. For the remaining experiments, the mixing ratios of HO_2 and NO are inferred from the rate of growth of H_2O_2 (detected as $H_2O_2{\cdot}CF_3O^-$, m/z 119), 2-methylpropene hydroxy hydroperoxide ($C_4H_{10}O_3{\cdot}CF_3O^-$, m/z 191) and 2-methylpropene hydroxy nitrate ($C_4H_9NO_4{\cdot}CF_3O^-$, m/z 220), using the procedure employed in the literature.[29,33,38] As such, the reference compound 2-methylpropene is used to infer NO and HO_2 mixing ratios which are then combined with rate coefficients for the crotonaldehyde hydroxy peroxy radicals to obtain the bimolecular lifetime of those peroxy radicals.

During oxidation, H_2O_2 is formed by:

$$HO_2 + HO_2 \rightarrow H_2O_2 + O_2$$

The production rate of H_2O_2 ($P_{H_2O_2}$) is thus given by:

$$P_{H_2O_2} = k_{HO_2+HO_2} \times [HO_2]^2 \tag{S8}$$

The HO_2 mixing ratio is determined from the observed rate of growth of H_2O_2 ($P_{H_2O_2}$) and the recommended rate coefficient for the reaction $k_{HO_2+HO_2}$ including a dependence on water vapor:[47]

$$[HO_2] = \sqrt{\frac{P_{H_2O_2}}{k_{HO_2+HO_2}}} \tag{S9}$$

$$\begin{aligned} k_{HO_2+HO_2} = &\left(2.2 \times 10^{-13} \exp\left(\frac{600}{T}\right) + 1.9 \times 10^{-33}[M] \exp\left(\frac{980}{T}\right)\right) \\ &\times \left(1 + 1.4 \times 10^{-21}[H_2O] \exp\left(\frac{2200}{T}\right)\right) \end{aligned} \tag{S10}$$

T in K, and concentrations in molecules cm^{-3}. In these experiments, the mixing ratio of NO is determined from the rate of growth of the 2-methylpropene hydroxy nitrate and hydroxy hydroperoxide. Specifically, the mixing ratio of HO_2, determined as above, is combined with the rate of growth of 2-methylpropene hydroxy hydroperoxide to infer the hydroxy peroxy radical mixing ratio. Based on this and the rate of growth of the 2-methylpropene hydroxy nitrate, the NO mixing ratio can be calculated:

$$[NO] = \frac{P_{RONO_2}}{P_{ROOH}} \frac{c_{ROOH}}{c_{RONO_2}} \frac{Y_{ROOH}}{Y_{RONO_2}} \frac{k_{RO_2+HO_2}}{k_{RO_2+NO}} [HO_2] \tag{S11}$$

P_{RONO_2} and P_{ROOH} are the observed rates of growth of the 2-methylpropene hydroxy nitrate and hydroxy hydroperoxide, respectively, in ncts s^{-1}; c_{ROOH} and c_{RONO_2} are

the calculated CIMS sensitivities in ncts pptv^{-1}; Y_{ROOH} is the fractional yield of hydroperoxides from the reaction of the 3-methylpropene hydroxy peroxy radicals with HO_2 and Y_{RONO_2} is the corresponding 2-methylpropene hydroxy nitrate yield from the reaction with NO; $k_{RO_2+HO_2}$ is the rate coefficient for the reaction of HO_2 with the 2-methylpropene hydroxy peroxy radical in cm^3 molecule^{-1} s^{-1} and k_{RO_2+NO} is the corresponding rate coefficient for the reaction with NO. The growth rates, P_{RONO_2} and P_{ROOH}, are determined from linear least-square fits to the signals as a function of time during the period with the lights on.

For the CIMS sensitivities of the 2-methylpropene hydroxy hydroperoxides and hydroxy nitrates, the average of the two structural isomers is used. The hydroperoxide yield (Y_{ROOH}) for the 2-methylpropene hydroxy peroxy radical reacting with HO_2 is assumed to be unity, as is the recommendation for simple peroxy radicals.[48–51] For the reaction with NO, the reported nitrate yield (Y_{RONO_2}) of 0.09 is used.[52]

The measured value (298 K) of 9.6×10^{-12} cm^3 molecule^{-1} s^{-1} is used for the bimolecular reaction of 2-methylpropene hydroxy peroxy radicals and NO.[53] For the reaction with HO_2, a bimolecular rate coefficient at 296 K of 1.48×10^{-11} cm^3 molecule^{-1} s^{-1} is used.[54] This is the IUPAC recommended value for the 2-OH,1-OO isomer and is assumed to be isomer independent.

S12 Importance of $RO_2 + RO_2$

Based on the observed growth of 2-methylpropene and crotonaldehyde hydroxy nitrates (m/z 220 and 234, respectively), the average NO mixing ratios (Section S11), the nitrate yields from RO_2 + NO (Section S16), the estimated CIMS sensitivities of the hydroxy nitrates (Section S8) and the rate coefficients of RO_2 + NO (Section S13), the average RO_2 mixing ratio during the oxidation can be inferred. This approach suggests that the average mixing ratios of 2-methylpropene and crotonaldehyde hydroxy peroxy radicals in the different experiments fall in the ranges $3 \times 10^{-3} - 10$ ppt and $2 \times 10^{-3} - 40$ ppt, respectively.

Recently, experimental rate coefficients for the reaction RO_2 + RO_2 $\rightarrow$ ROOR + O_2 were published for a range of peroxy radical with varying size and degree of oxidation.[46] A rate coefficient of 1.3 $\times10^{-12}$ cm^3 molecule^{-1} s^{-1} was found for the self-reactions of both $CH_3C(O)CH_2O_2$ and HO-$C_4H_8O_2$, which are the peroxy radicals most closely resembling the crotonaldehyde peroxy radicals studied here.[46] By combining this rate coefficient with the inferred peroxy radical mixing ratios, we can estimate the importance of RO_2 + RO_2 for the experiments. The inferred RO_2 mixing ratios correspond to pseudo-first-order rate coefficients for RO_2 + RO_2 in the range $1 \times 10^{-7} - 1 \times 10^{-3}$ s^{-1}. For comparison, the pseudo-first-order rate coefficients for reactions with NO in the different experiments are in the range $9 \times 10^{-3} - 3 \times 10^{2}$

s^{-1} and $2 \times 10^{-2} - 3 \times 10^{2}$ s^{-1} for the 2-methylpropene and crotonaldehyde hydroxy peroxy radicals, respectively. The pseudo-first-order rate coefficients for the reaction with HO_2 are up to 0.1 s^{-1}. In the high-NO experiments, the HO_2 mixing ratio cannot be assessed, thus a lower limit can not be given for the pseudo-first-order rate coefficients with HO_2. For the crotonaldehyde hydroxy peroxy radicals, the RO_2 + RO_2 reaction also competes with the unimolecular H-shifts with an experimental rate coefficient of 4×10^{-2} s^{-1} for the isomer with the slowest reaction. These estimates suggest that RO_2 + RO_2 account for less than 0.3 % of the reactivity in all experiments and typically much less.

Berndt et al. showed that for larger, more highly oxidized peroxy radicals, the rate coefficient for RO_2+RO_2 could be much faster with values up to 2.6×10^{-10} cm^3 $molecule^{-1}$ s^{-1}. If RO_2+RO_2 did account for a significant fraction of the total peroxy radical reactivity and this reaction is not considered, it would lead to an overestimation of the bimolecular lifetime for a given experiment and result in determined H-shift rate coefficients that were too slow, assuming the 2-methylpropene and crotonaldehyde hydroxy peroxy radicals react with other RO_2's with the same rate coefficients. However, even using this upper limit rate coefficient for the RO_2+RO_2 reactions increases the experimentally determined peroxy radical H-shift rate coefficients by only 30 - 40 % for the different isomers compared to neglecting this reaction pathway. A rate coefficient for RO_2+RO_2 of 8.7×10^{-11} cm^3 $molecule^{-1}$ s^{-1} (1/3 of the fastest measured rate coefficient) is necessary to increase the rate coefficients determined here by about 10 %. Any possible effect of RO_2+RO_2 on the observed stereoselectivity cannot be assessed, as we do not know if the diastereomers may react bimolecularly with significantly different rate coefficients.

An additional effect that is also difficult to assess is the influence of different RO_2+RO_2 rate coefficients for the 2-methylpropene and crotonaldehyde hydroxy peroxy radicals. As 2-methylpropene forms mostly tertiary peroxy radicals, it is expected to react more slowly in RO_2+RO_2 reactions, which would decrease the normalized crotonaldehyde yields.[55] This would in turn lead to an overestimation of the observed rate coefficients, working to counteract the effect on the bimolecular lifetime. However, as discussed in the initial paragraph in this section, it seems unlikely than any of the peroxy radicals formed here will react rapidly enough by RO_2+RO_2 for this reaction to matter.

S13 Simple Chemical Model to Obtain Experimental H-shift Rate Coefficients

The experimental H-shift rate coefficients are obtained by least square fit of the experimental results to results from a simple chemical model with the H-shift rate as the variable. The model includes the following parameters:

- $k_{CRALD+OH} = 3.49 \times 10^{-11}$ cm^3 molecule^{-1} s^{-1} at 296 K.[56] This experimentally determined literature value is in good agreement with earlier experimental determinations.[57,58]

- $k_{2-me-prop+OH} = 5.20 \times 10^{-11}$ cm^3 molecule^{-1} s^{-1}.[59]

- $[OH] = 2 \times 10^6$ molecules^{-1} cm^3. The model results are not sensitive towards this value, as the important model output is the ratio between products from crotonaldehde and 2-methylpropene.

- $Y_{CRALD-addition} = 0.56$. 56 % yield of OH addition in the reaction of crotonaldehyde and OH based on SAR results.[56,57] Literature experimental results suggest that addition and abstraction are comparable, but are unable to constrain the branching further.[56,60]

- $Y_{2-Me-prop-prim-addition} = 0.89$. Yield of primary OH-addition to 2-methylpropene. Experimental value.[52]

- $Y_{CRALD-HN} = 0.017$. Hydroxy nitrate yield for the reaction of crotonaldehyde hydroxy peroxy radicals with NO. Based on best fit to the high-NO experiments. This value is in excellent agreement with the experimental value between 0.16 and 0.19 determined here (Section S16).

- $Y_{2-Me-prop-HN} = 0.09$. Hydroxy nitrate yield for the reaction of 2-methylpropene hydroxy peroxy radicals with NO. Experimental value.[52]

- $T = 296$ K.

- $k_{2-me-prop-OH-OO-isom} = 8.8 \times 10^{-5}$ s^{-1}. Summed rate of unimolecular H-shifts for 1-OH,2-OO-2-methylpropene. Based on calculated values (Table S3).

- $k_{CRALD-OH-OO+NO} = 8.8 \times 10^{-12}$ cm^3 molecule^{-1} s^{-1}. Based on parametrization of experimental values.[28]

- $k_{2-me-prop-OH-OO+NO} = 9.6 \times 10^{-12}$ cm^3 molecule^{-1} s^{-1}. Experimental value.[53]

- CIMS sensitivities of the various hydroxy nitrates as given in Table S15.

- The rate coefficients of the unimolecular H-shifts of the crotonaldehyde hydroxy peroxy radicals represent the variable in the model and are determined by least-square fits of the chemical model to the experimental data. For comparison between experiments and calculations, the model is also run using the MC-TST calculated values for the aldehydic H-shifts.

S14 Uncertainty in the Experimental Reaction Rate Coefficients

The uncertainty in the experimentally determined reaction rate coefficients is estimated as previously described.[29,38] The total uncertainty depends on the uncertainties in both the measured peak area ratios and the inferred bimolecular lifetime.

S14.1 Uncertainty in Peak Area Ratio

The uncertainty in the peak area ratio is determined as the propagated total uncertainty from the standard deviation in peak area from the three repeated GC's, the standard deviation in the peak area fitting parameters, and the standard deviation in the peak area ratio from the high-NO experiments. The uncertainty in the peak area fitting parameters is determined from Monte Carlo simulation including 10,000 fits with the peak parameters (width and exponential-decay parameter) of CRALD HN and 2-Me-prop HN covaried from the determined optimal value by up to 40 % in each direction using uniformly distributed random numbers. Fits that have deteriorated by more than 2 standard deviations from the average are discarded. The standard deviation of the peak area ratio of the included fits is assigned to the standard deviation of the peak fitting parameters. Test using 11,000 trials yield the same results, suggesting that the values have converged. One fit is done for the high-NO experiments ([NO] > 100 ppb) and one is done for the low-NO experiments. Each of these is then applied to all points within that group. This is not possible for the three slightly overlapping crotonaldehyde hydroxy nitrate peaks, as the relatively large variations of the peak parameters causes the fitting tool to incorrectly assign the three individual peaks. Thus, it is done for only the fourth (more separated) peak and the same standard deviation from the peak fitting parameters is assigned to the peak ratio of all four crotonaldehyde hydroxy nitrate peaks.

Due to the use of an external reference (2-methylpropene), additional uncertainty is assigned to the peak area ratio to account for potential variations in the ratio of the two components of the mixture over time. As an upper limit for the uncertainty from this, we use the standard deviation of the peak ratio from all the high-NO experiments for each peak.

S14.2 Uncertainty in Bimolecular Lifetime

Uncertainty in the determined bimolecular lifetime is estimated differently for the high-NO and low-NO experiments, due to differences in the ways the bimolecular lifetime is calculated for the two sets of experiments.

For the high-NO experiments, the bimolecular lifetime is determined from the measured initial NO concentration and the rate coefficient for CRALD-OH-OO with NO.

We estimate the uncertainty in the measured initial NO concentrations to be about 20 % and the uncertainty for CRALD + NO to be about 10 % based on the small variation between different alkyl and oxygenated (non-acyl) peroxy radicals.[53,61]

For the low-NO experiments, the bimolecular lifetime is based on the inferred NO and HO_2 concentrations (see Equations S11 and S9) determined from the products of 2-methylpropene and the rate coefficients for CRALD-OH-OO with NO and HO_2. For the production rate of the 2-methylpropene hydroxy nitrate and hydroperoxide, we use the standard 1σ of the linear least-square fits of the signal as a function of time during oxidation. The associated calculated CIMS sensitivities are each assigned a default uncertainty of 30 %.[29,38] For $k_{HO_2+HO_2}$, we use the assigned uncertainty of 15 %.[29,47] For the hydroperoxide yield for 2-methylpropene-OH-OO+HO_2, we assign an uncertainty of 5%,[47,62] while the nitrate branching for 2-methylpropene-OH-OO+NO has a stated uncertainty of 11%.[52] Finally, for the rate coefficient for the reaction of the crotonaldehyde hydroxy peroxy radicals with HO_2, we use a standard deviation of 25 % estimated from the RMSE of the fit to experimental data in Wennberg et al.[28]

S14.3 Total Uncertainty

From the determined uncertainty of each experimental data point, the total uncertainty in the experimental reaction rate coefficient is determined using a Monte Carlo approach. 5000 data sets are generated by shifting each point within its uncertainty in the x and y dimension using uniformly distributed random numbers. For each new data set, the best fit is calculated by minimizing the linear least square deviation of the modeled values to the experimental. The total uncertainty in the experimental rate coefficient is the full width spanned by the 5000 fits.

S15 3-Hydroxybutanal Oxidation

To aid the assignment of the m/z 234 peaks in the crotonaldehyde oxidation, experiments were conducted using 3-hydroxybutanal. As shown in Figure S10, this should yield the two stereoisomers of the hydroxy nitrate isomer expected to be the major product of crotonaldehyde oxidation (3-OH,2-ONO_2-CRALD) and thus only two m/z 234 GC peaks.

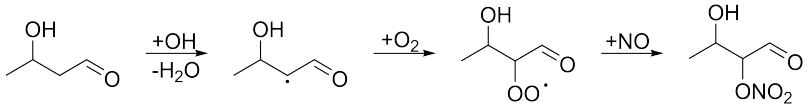

Figure S10: OH initiated oxidation of 3-hydroxybutanal leading to hydroxy nitrate formation.

Surprisingly, in the GC of 3-hydroxybutanal, we see the same four peaks as observed in crotonaldehyde oxidation. However, as shown in Figure S11, the intensity

of the two later-eluting relative to the two earlier-eluting peaks is larger in the 3-hydroxybutanol oxidation compared to the crotonaldehyde oxidation. We therefore assign these to arise from the 3-OH,2-ONO2 diastereomers. However, the two initial smaller peaks are only slightly less intense in the chromatogram of 3-hydroxybutanal compared to crotonaldehyde. For pure 3-hydroxybutanal, these peaks should not be observed. Unfortunately, 3-hydroxybutanal was available only as "technical grade", whose purity could not be verified from the supplier. However, a single peak at m/z 173 (hydroxybutanal + CF_3O^-) before any reactions suggests that the additional peaks are not due to impurities of 2-hydroxybutanal, assuming the two are separable with the chromatographic setup employed.

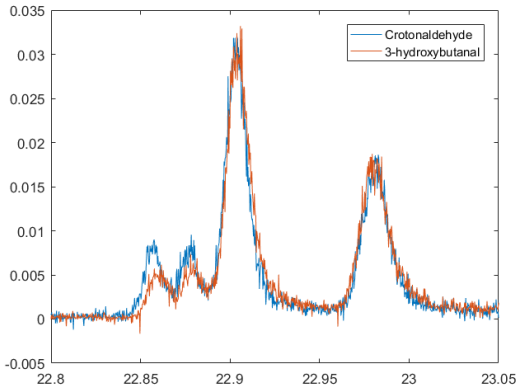

Figure S11: Comparison of the chromatograms (m/z 234) obtained in high-NO experiments with crotonaldehyde and 3-hydroxybutanal. The 3-hydroxybutanal chromatogram is scaled to the tall peaks from crotonaldehyde oxdation.

A likely explanation for the observed chromatogram is the presence of crotonaldehyde in the sample. Being a β-hydroxy alcohol, dehydration is a likely reaction of 3-hydroxybutanal.[63] As shown in Figure S12, this would lead to crotonaldehyde. Crotonaldehyde could be present in the purchased sample or formed during evaporation into the chamber. The presence of crotonaldehyde would explain why all four peaks are observed, while the higher relative abundance of the two later-eluting peaks are due to the 3-hydroxybutanal. Due to the double bond in crotonaldehyde, it is expected to react significantly faster with OH than 3-hydroxybutanal.[64] This means that even relatively small amounts of impurities could significantly affect the chromatogram.

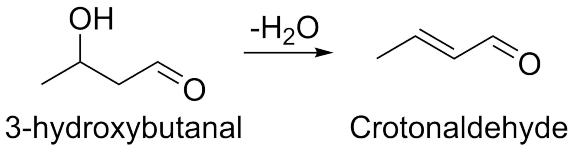

Figure S12: Aldol condensation of 3-hydroxybutanal forming crotonaldehyde.

S16 Hydroxy Nitrate Yield

The overall hydroxy nitrate yield for the crotonaldehyde hydroxy nitrates are estimated from the high-NO experiments where it can be assumed that all hydroxy peroxy radicals react with NO. It is determined relative to the HN yield of 2-methylpropene hydroxy peroxy radicals from both the direct CIMS sampling the the GCs. From the published HN yield of the 2-methylpropene of 0.09, the absolute CRALD HN yield can be estimated.[52] For both approaches, the results for the different high-NO experiments are averaged, but show little variation.

For the direct sampling, the background-corrected m/z 234 (CRALD-HN) signal is compared to the corresponding m/z 220 (2-Me-prop-HN) signal. The signals are corrected for the isomer-weighted CIMS sensitivities (Table S15), the 1:10 2-methylpropene:crotonaldehyde ratio in the gas mixture, 56 % OH-addition to CRALD (Section S13)[56,57] and slight differences in the rate coefficients for reaction of the peroxy radicals with NO (Section S13). This approach yields an overall HN yield of the crotonaldehyde hydroxy peroxy radicals of 1.9 %.

A similar approach is used to estimate the value from the gas chromatograms of the high-NO experiments. The fitted area of each HN peak is corrected by the corresponding CIMS sensitivity and all peaks corresponding to CRALD HN and 2-me-prop HN, respectively, are summed. The ratio of these peaks is corrected as above by for the difference in peroxy radical abundance and reaction rate with NO. This approach yields a CRALD HN yield of 1.6 %, in good agreement with the direct sampling approach.

A parametrization for the nitrate yield from the reaction of a peroxy radical with NO was recently published.[28] For simple peroxy radicals at 293 K and 993 hPa, the nitrate yield, α_0, is given by:

$$\alpha_0 = (0.045 \pm 0.016)n - (0.11 \pm 0.05) \tag{S12}$$

where n is the number of non-hydrogen atoms excluding the peroxy moiety. For the CRALD hydroxy peroxy radicals, $n = 6$ suggesting a nitrate yield of 16 % using this simple approximation. However, it was noted that for multifunctional compounds, the nitrate yield was generally lower.[28] While corrections for this is poorly constrained,

estimated factors were given to be multiplied by α_0. The nitrate yield of α carbonyl peroxy radicals is reduced by 90 % and the nitrate yield of β carbonyl peroxy radicals by 45 %. Similarly, β hydroxy peroxy radicals have a nitrate yield reduced by 10 % and γ hydroxy groups reduce the nitrate yield by 5 %. With these corrections, the parametrization suggests a nitrate yield of 7.9 % and 1.4 % for 2-OH,3-OO and 3-OH,2-OO, respectively. As 3-OH,2-OO is the dominant structural isomer, these values seem consistent with the overall experimental value obtained here.

S17 Chromatograms

Figure S13 shows the four crotonaldehyde hydroxy nitrate peaks (m/z 234) along with the two 2-methylpropene hydroxy nitrate peaks (m/z 220). The latter of the 2-methylpropene hydroxy nitrate peaks (retention time of 8 minutes) is used to normalize the m/z 234 signals. 2-methylpropene serves as a reference to account for differences in OH and NO reactivity between experiments.

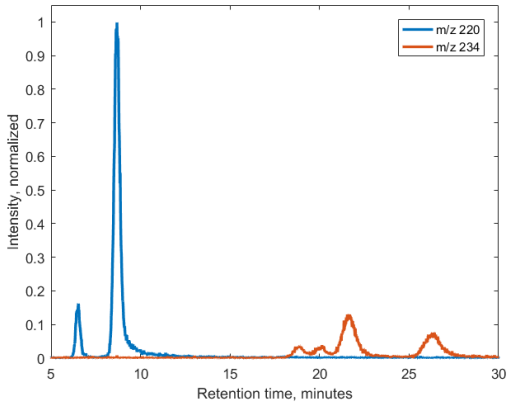

Figure S13: Chromatograms of m/z 220 (2-methylpropene hydroxy nitrate·CF_3O^-) and m/z 234 (crotonaldehyde hydroxy nitrate·CF_3O^-). The intensity of the chromatograms have been normalized to the intensity of the second 2-methyl hydroxy nitrate peak.

For the hydroxy nitrates produced from 2-methylpropene, two peaks are observed at m/z 220 (see Figure S13) consistent with the two structural isomers of the hydroxy nitrates clustered with CF_3O^-, as observed before.[52] These have previously been assigned with the larger (later-eluting) peak corresponding to external OH-addition. This assignment is confirmed by the growth of the first of these peaks in the dark under NO_3-dominated conditions, as NO_3 strongly favors external addition (see Section S18).[65] The retention times of the 2-methylpropene hydroxy nitrate peaks are 6 and 8 minutes, respectively, under the experimental conditions employed here. It is the latter of these two peaks that serves as the reference signal to normalize the CRALD peak areas to account for differences in OH and NO reactivity between experiments.

S18 NO_3 Experiment

From consecutive gas chromatograms recorded after the lights have been turned off, the initial m/z 220 peak is observed to increase over time in experiments with low NO (Figure S14, left panel). The same growth is not observed for the second m/z 220 peak. The two m/z 220 peaks are assigned to the two structural isomers of 2-methyl hydroxy nitrate clustered with CF_3O^-, with the first peak corresponding to the primary nitrate.[52] The observed growth of the primary nitrate after the lights have been turned off is consistent with oxidation by NO_3. This conclusion is substantiated by the fact that this growth is not observed in experiments with high initial NO mixing ratios (Figure S14, right panel), where NO_3 formation is expected to be negligible.

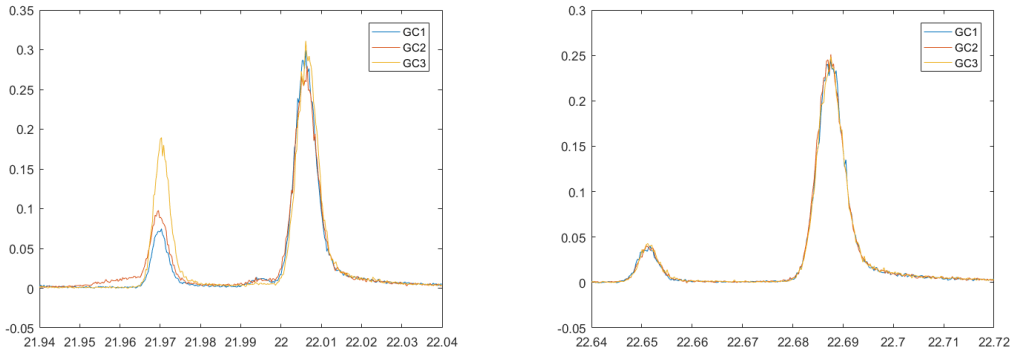

No initial NO

443 ppb initial NO

Figure S14: Comparison of the m/z 220 (2-methylpropene hydroxy nitrate·CF_3O^-) signal in three consecutive GCs of the same reaction mixture after the lights have been turned off. The left panel is from an experiment with no initial NO added, while the right panel is from an experiment with a high initial NO mixing ratio (457 ppb).

To assess the NO_3 chemistry, an additional experiment was performed. The NO_3 chemistry was probed by adding NO_2 and O_3 to the mixture of crotonaldehyde and 2-methylpropene in the chamber in the dark. This leads to formation of NO_3 by:

$$O_3 + NO_2 \rightarrow O_2 + NO_3 \tag{S13}$$

NO_2 was added before O_3 and in great surplus to limit ozonolysis. The lack of UV light means that no OH radicals are formed from photolysis and NO_3 is thus the main reactant. As shown in Figure S15, this leads to a significantly different relative ratio of the two m/z 220 peaks compared to the high-NO experiment. In the high-NO_3 experiment, virtually only the first 2-methylpropene hydroxy nitrate peak is observed. This peak has previously been assigned to the primary nitrate, which is consistent with the strong terminal-addition preference of NO_3.[52,65] This suggests that the second 2-methyl HN peak is not formed from NO_3-chemistry and that this peak can thus be used as a reference for the unimolecular chemistry. As shown in

the second panel of Figure S15, it appears that none of the crotonaldehyde hydroxy nitrates are formed in significant amounts by NO_3-addition and that this reaction is thus not problematic for our rate determination. The lack of observed growth of crotonaldehyde HN may be explained by the observation that the NO_3-addition is at least about a factor of 10 and likely about a factor of 100 slower for crotonaldehyde compared to 2-methylpropene.[66,67]

Instead, in the high-NO_3 experiment, a significant single peak of m/z 236 is observed. This mass is consistent with the 2-methylpropene nitroso hydroperoxide clustered with CF_3O^-. This compound is observed in only negligible amounts in the high-NO experiment (right panel, Figure S15).

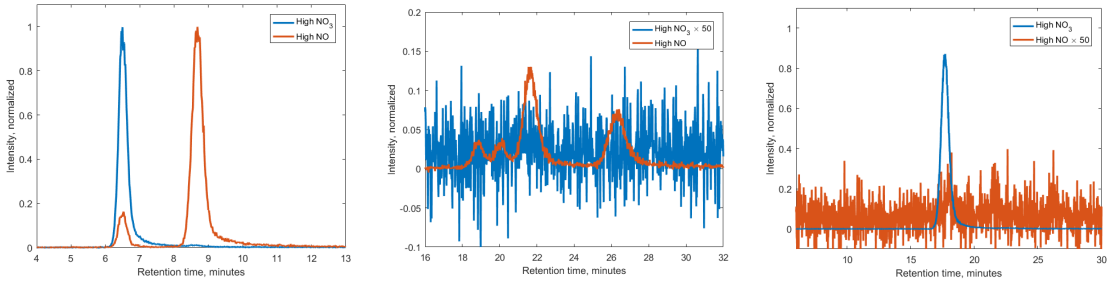

m/z 220 m/z 234 m/z 236

Figure S15: Chromatograms comparing experiments conducted with a high mixing ratio of NO_3 and NO. The signals are normalized to the most intense m/z 220 peak and for the m/z 234 and m/z 236 chromatograms, the high-NO_3 and high-NO chromatograms, respectively, have been further multiplied by a factor of 50.

S19 Branching for OH-addition

The relative importance of the two OH-addition pathways in crotonaldehyde is assessed from the high-NO experiments (blue trace in Figure 3) and the calculated CIMS sensitivities of the formed hydroxy nitrates, assuming each has the same nitrate yield. As observed for the two smaller peaks eluting first, we expect the two diastereomers to be formed in equal amounts, as they are formed by O_2-addition to a (near-)planar alkyl radical.[68] The fact that the signal of the last-eluting crotonaldehyde hydroxy nitrate is almost a factor of two smaller than the other major hydroxy nitrate (when including estimated CIMS sensitivity, see Table S15) is attributed to a lower GC transmission due to its longer retention time. We estimate the branching between the two addition pathways to be about 10:90 favoring addition at the 3-position. This assumes that the abundance related to the fourth peak is equal to that of the third and that the nitrate yield is the same for all four peroxy radicals.

Earlier results based on FT-IR measurements with high NO concentrations suggest that addition to the 2-position may be as high as 40 % of the total addition pathway.[60]

However, this suggestion was sensitive to speculation about the most likely bond-scission product for a specific alkoxy radical, which our calculations show are likely not valid (Section S20) - a possibility also noted by the authors.[60] Specifically, our calculation suggest that scission of the $CH_3CH(OH)CH(O)CHO$ alkoxy radical is fastest towards the CH(OH)-group rather than the CHO-group, which is opposite from what is observed for methacrolein and methylvinylketone.[69–72] This trend is in agreement with our calculations for those systems (see Section S7) and likely stem from the greater stability of the CH_3CHOH leaving group in crotonaldehyde compared to the CH_2OH leaving group for the other alkoxy radicals. On the other hand, the assumption that the nitrate yield is the same for the two structural isomers is likely also not correct: Though poorly constrained, experimental results for other compounds suggest that the positions of the functional groups would lead to a lower nitrate yield in for the 3-OH,2-OO-CRALD hydroxy peroxy radicals compared to the 2-OH,3-OO-CRALD hydroxy peroxy radicals (see Section S16).[28,72] This would suggest an even larger preference for 3-OH addition.

S20 High-NO Oxidation Mechanism

Two earlier studies have investigated the OH-initiated oxidation of crotonaldehyde under high-NO conditions using Fourier transform infrared (FT-IR) spectroscopy and gas chromatographs with flame ionization (FID), photoionization (PID) and electron capture detectors (ECD).[56,60] Both studies find that, under high-NO conditions, the major organic products are acetaldehyde, glyoxal and an unsaturated PAN species. While the CF_3O^--CIMS employed here is not highly sensitive to these products, we do see growth of signals consistent with the CF_3O^- adducts of these (m/z 129, 143 and 232, respectively) during the oxidation under high-NO conditions, but also in an experiment designed to identify products formed without added NO (Figure S17). However, the major signal observed growing in is m/z 159 consistent with 2-hydroxy propanal ($C_3H_6O_2 \cdot CF_3O^-$). 2-hydroxy propanal is proposed as a possible product in Magneron et al.[56] and consistent with the theoretical mechanism outlined in Section S20. Our calculations predict the same products from OH-addition as observed in the earlier experimental studies, but with somewhat different yields.[56,60]

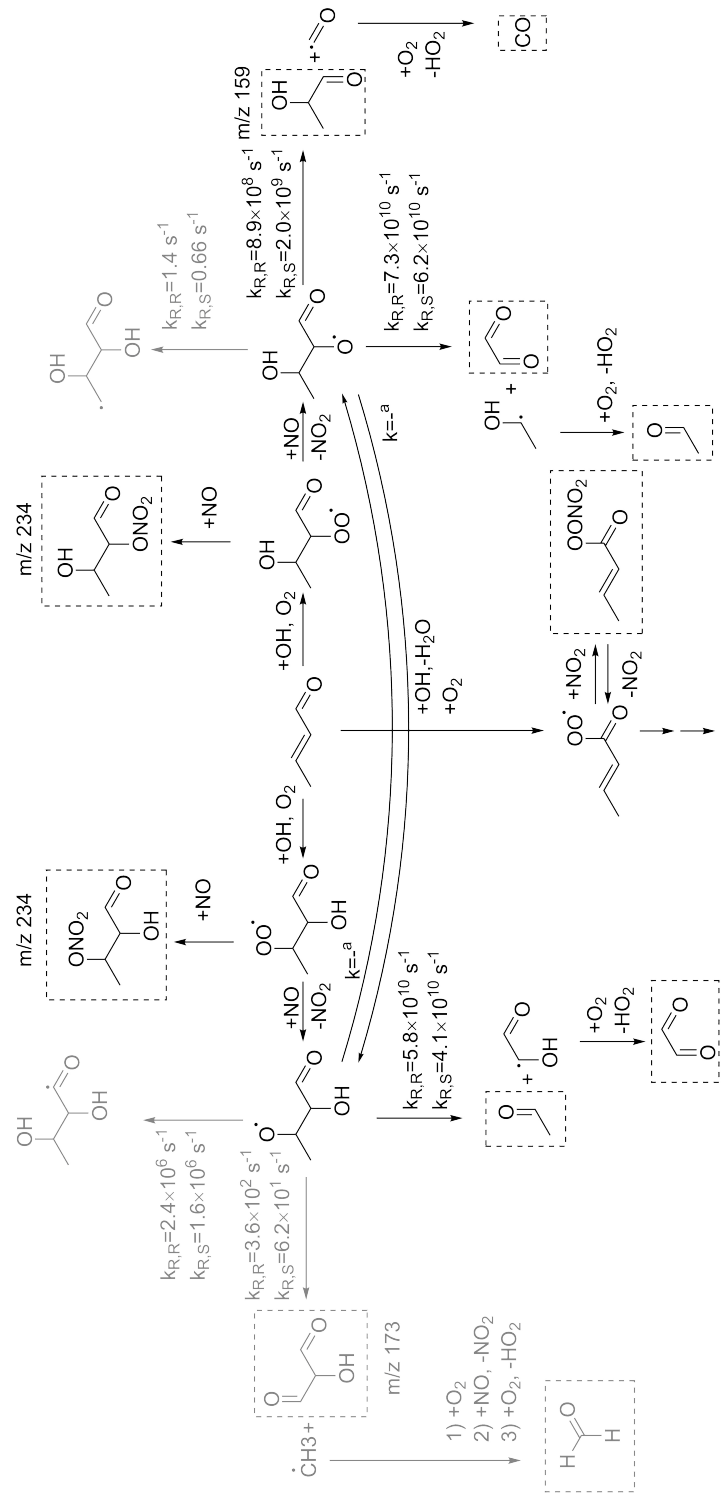

Figure S16: Proposed high-NO oxidation mechanism of crotonaldehyde. The rate coefficients given are calculated using the approach by Møller et al., but without the F12 single-point calculations at 298.15 K. Due to the very low barrier heights for the fastest reactions, the rate coefficients may not be accurate for those. Pathways in grey are unlikely based on the calculations. Closed-shell products are identified by a dashed square and m/z are given for their complex with CF_3O^- for the compounds we expect to be sensitive to. Reaction pathways following H-abstraction (center) have not been calculated here, but several options are given in the literature.[56,60] [a] Attempts at optimizing this TS decompose to the products of the fast alkoxy bond scission.

Based on the measured products, it has been proposed that about 40 % of the OH-addition to crotonaldehyde may occur at the 2-position.[60] This conclusion, however, hinges on the glyoxal yield and the assumption that reaction of the alkoxy radical

2-O,3-OH (in Figure S16) to yield 2-hydroxy propanal (m/z 159) dominates over the reaction to yield glyoxal (m/z 143). As Orlando and Tyndall argue, if the opposite is the case (as our calculations suggest), the addition at the 2-position is less than the suggested 40 %, and thus closer to the ~10 % estimated here.
Figure S17 shows growth of m/z 129, 143 and 232 during oxidation. These masses are consistent with the CF_3O^--adducts of acetaldehyde, glyoxal and an unsaturated PAN species, which are all proposed to be major products of the NO-dominated chemistry of crotonaldehyde+OH in previous literature[56,60] and our theoretical model in Figure S16. The chemical compositions are confirmed by high mass resolution analysis, although the m/z 143 signal seems to be comprised of two different compounds in comparable amounts. However, as these are all compounds we do not expect to be sensitive towards, they may be other compounds of the same composition.

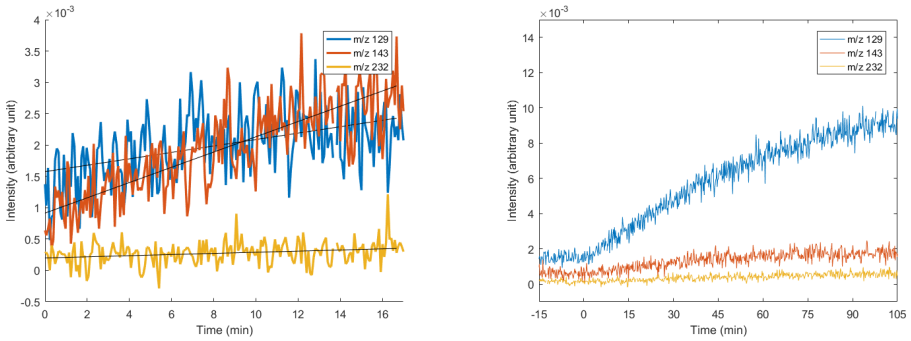

Figure S17: Growth during oxidation of selected m/z under high-NO conditions. Oxidation is initiated by turning on the light at time = 0 min. Left panel: 10:1 mixture of crotonaldehyde and 2-methylpropene with $[NO]_{initial}$ = 581 ppb. Right panel: Crotonaldehyde only with no added NO. Note the difference in oxidation time.

S21 Oxidation Mechanism Following Aldehydic H-shifts

At long bimolecular lifetime, several peaks of m/z 175 are observed that are not present in either the high-NO or high-HO_2 experiments suggesting that these are products of the unimolecular chemistry (see Figure S20). High mass resolution analysis suggest some of these peaks correspond to the chemical composition $C_3H_6O_3 \cdot CF_3O^-$. One compound consistent with this is 2-hydroperoxy propanal, a product of the aldehydic H-shift in 3-OO,2-OH-CRALD followed by CO-loss, which could be competitive with O_2-addition (see Figure S18).[37] Surprisingly, the high mass resolution data do not suggest that any of the peaks correspond to the C_2 aldehyde peroxy acid ($C_2H_2O_4$), which the theoretical mechanism (Figures S18 and S19) predicts to be the major product of the unimolecular chemistry followed by alkoxy chemistry for both structural isomers. A potential explanation would be that it decomposes.

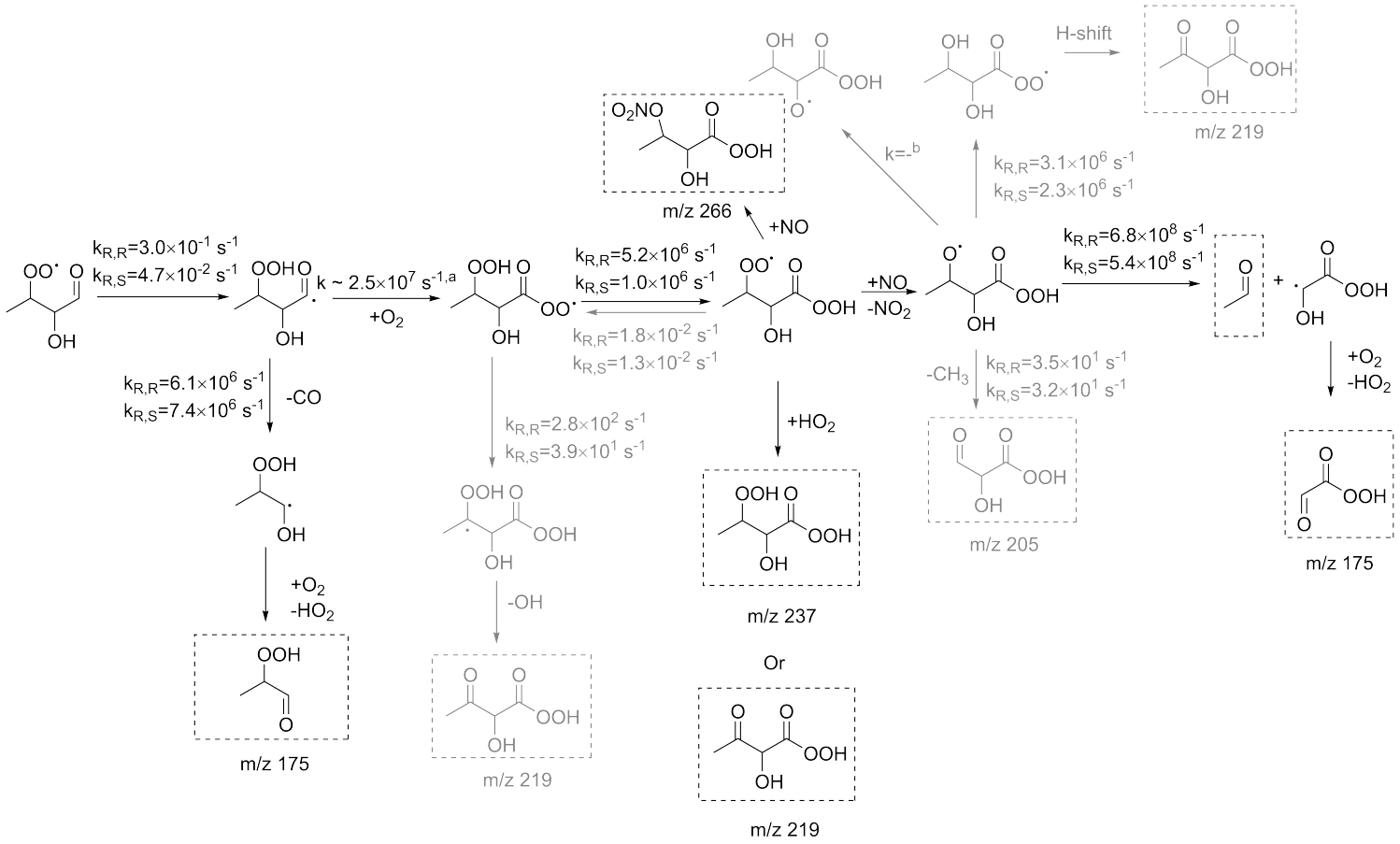

Figure S18: Proposed oxidation mechanism following the 1,5 aldehydic H-shift in 2-OH,3-OO-CRALD. The rate coefficients given are calculated using the approach by Møller et al., but without the F12 single-point calculations at 298.15 K. Due to the very low barrier heights for the fastest reactions, the rate coefficients may not be accurate for those. Pathways in grey are unlikely based on the calculations. Closed-shell products are identified by a dashed square and m/z are given for their complex with CF_3O^- for the compounds we expect to be sensitive to. [a] Estimated using an O_2-concentration of 0.2 bar and a bimolecular rate coefficient of 5×10^{-12} cm^3 molecule^{-1} s^{-1}.[73] [b] Attempts at optimizing this TS decompose to the products of the fast alkoxy bond scission (in black).

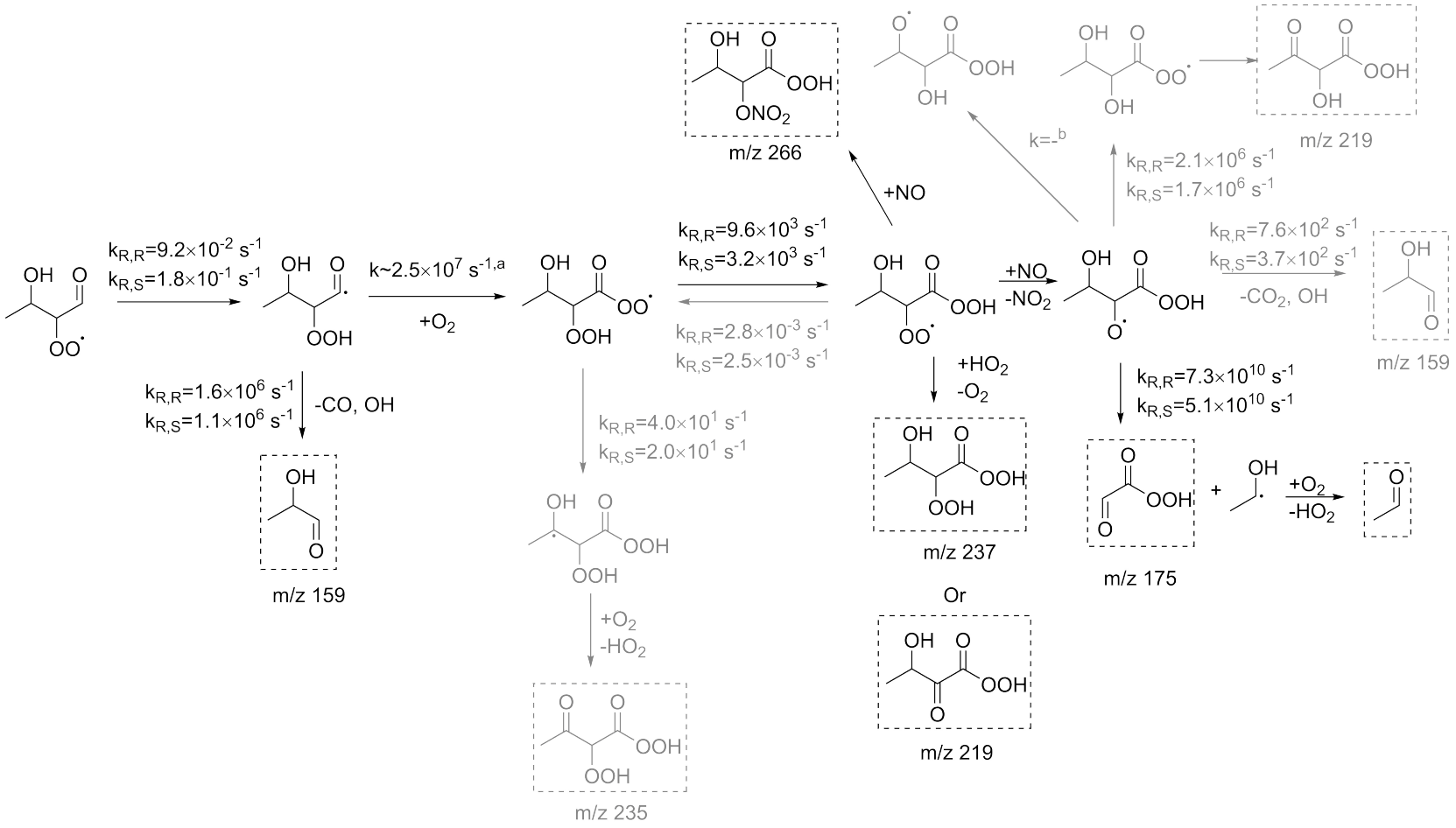

Figure S19: Proposed oxidation mechanism following the 1,4 aldehydic H-shift in 3-OH,2-OO-CRALD. The rate coefficients given are calculated using the approach by Møller et al., but without the F12 single-point calculations at 298.15 K. Due to the very low barrier heights for the fastest reactions, the rate coefficients may not be accurate for those. Pathways in grey are unlikely based on the calculations. Closed-shell products are identified by a dashed square and m/z are given for their complex with CF_3O^- for the compounds we expect to be sensitive to. [a] Estimated using an O_2-concentration of 0.2 bar and a bimolecular rate coefficient of 5×10^{-12} cm^3 molecule^{-1} s^{-1}.[73] [b] Attempts at optimizing this TS decompose to the products of the fast alkoxy bond scission (in black).

The reaction mechanisms following the unimolecular aldehydic H-shift (Figures S18 and S19) both predict compounds with m/z 175 to be major products via CO-loss or alkoxy bond scission. As shown in Figure S20, the chromatograms of m/z 175 differ significantly between experiments conducted with high NO, high HO_2 and with low mixing ratios of both leading to long bimolecular lifetimes. While one of the observed peaks (retention time of 2.3 minutes) seems to be a product of HO_2-chemistry, at least two of the observed peaks do not seem to correlate with products observed in the other two experiments suggesting that these are products of the unimolecular chemistry. This is in line with the calculated mechanisms. The peak with retention time of 4.5 minutes seems to have a small formation rate in the high HO_2-experiment, though it is difficult to assess.

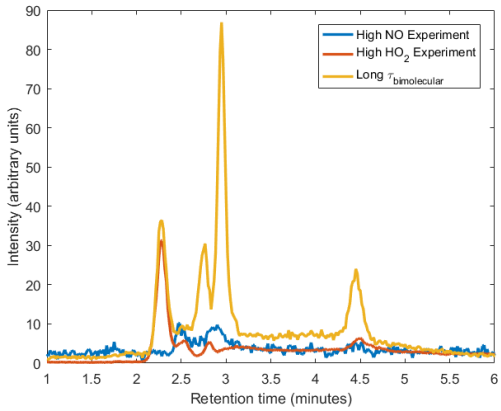

Figure S20: Chromatogram of m/z 175 following a high-NO experiment, a high-HO_2 experiment and an experiment with long bimolecular lifetime. The intensity is scaled to the summed GC areas of the 2-methylpropene hydroxy hydroperoxide (m/z 191) and the second 2-methylpropene hydroxy nitrate peak (m/z 220) to account for differences in OH exposure.

High mass resolution data ($(m/z)/\Delta(m/z) \sim 3500$) suggest that the first of the four peaks observed at long bimolecular lifetime is consistent with a chemical composition of $C_4H_{10}O_2 \cdot CF_3O^-$ and the remaining three peaks correspond to a chemical composition of $C_3H_6O_3 \cdot CF_3O^-$.

$C_4H_{10}O_2$ is consistent with the diol of 2-methylpropene. This potential assignment is corroborated by the fact that it is formed under high-HO_2 conditions, but not high-NO conditions and the fact that it is not preset in an experiment without 2-methylpropene (Figure S21). $C_3H_6O_3$ is consistent with the C3 hydroperoxy aldehyde formed by CO-loss and reaction with O_2 from the product of the 1,5 aldehydic H-shift in 2-OH,3-OO CRALD (Figure S18) and one of the peaks thus likely represents this compound. The second peak in the long-lifetime chromatogram in S20 is also not present in the the experiment with only crotonaldehyde (Figure S21) and is thus also likely formed from 2-methylpropene.

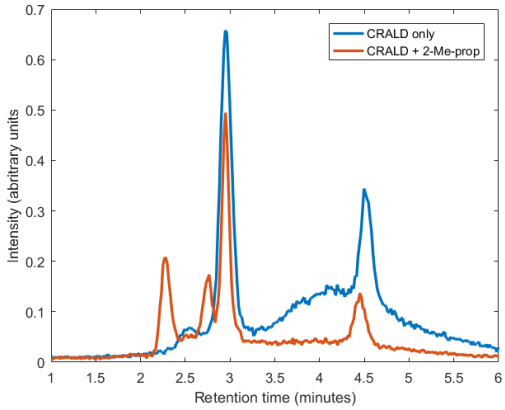

Figure S21: Chromatogram of m/z 175 without added NO in an experiment with only crotonaldehyde (CRALD only) and the 10:1 mixture of crotonaldehyde and 2-methylpropene (CRALD + 2-Me-prop).

S22 Crotonaldehyde Peak Area Ratios

Table S17: Bimolecular lifetime (τ_{bi}, in s) and gas-chromatograph peak areas of each of the four crotonaldehyde hydroxy nitrate peaks divided by the peak area of the second 2-methylpropene hydroxy nitrate peak. Each value is the average of the ratio form three consecutive GCs. The values do not take into account the determined CIMS sensitivities (Table S15). Peak 1 is *(R*,S*)*-2-OH,3-ONO_2−CRALD, Peak 2 is *(R*,R*)*-2-OH,3-ONO_2−CRALD, Peak 3 is *(R*,R*)*-3-OH,2-ONO_2−CRALD and Peak 4 is *(R*,S*)*-3-OH,2-ONO_2−CRALD. At long bimolecular lifetimes, the area of Peak 2 was too small to be fitted, indicated by a "-".

Expt.	τ_{bi}	Peak 1	Peak 2	Peak 3	Peak 4
A	2.15×10^{0}	5.58×10^{-2}	1.54×10^{-2}	1.45×10^{-1}	6.63×10^{-2}
B	2.81×10^{0}	3.68×10^{-2}	1.70×10^{-2}	1.44×10^{-1}	6.77×10^{-2}
C	1.00×10^{-2}	4.89×10^{-2}	4.18×10^{-2}	2.58×10^{-1}	1.81×10^{-1}
D	1.66×10^{1}	3.84×10^{-2}	-	5.59×10^{-2}	3.24×10^{-2}
E	8.72×10^{-3}	5.88×10^{-2}	5.12×10^{-2}	3.11×10^{-1}	2.27×10^{-1}
F	6.07×10^{0}	4.59×10^{-2}	9.13×10^{-3}	1.08×10^{-1}	4.67×10^{-2}
G	7.82×10^{0}	4.00×10^{-2}	-	8.30×10^{-2}	3.36×10^{-2}
H	3.76×10^{-3}	5.18×10^{-2}	4.28×10^{-2}	2.55×10^{-1}	1.88×10^{-1}
I	4.64×10^{0}	4.68×10^{-2}	1.32×10^{-2}	1.53×10^{-1}	8.92×10^{-2}
J	8.65×10^{-3}	5.28×10^{-2}	4.82×10^{-2}	2.77×10^{-1}	1.98×10^{-1}
K	3.83×10^{1}	1.51×10^{-2}	-	2.13×10^{-2}	9.72×10^{-3}
L	6.71×10^{1}	7.54×10^{-3}	-	2.39×10^{-2}	1.96×10^{-2}
M	3.73×10^{1}	1.24×10^{-2}	-	1.47×10^{-2}	6.69×10^{-3}
N	7.91×10^{-3}	5.22×10^{-2}	4.45×10^{-2}	2.77×10^{-1}	1.98×10^{-1}

References

[1] Møller, K. H.; Otkjær, R. V.; Hyttinen, N.; Kurtén, T.; Kjaergaard, H. G. Cost-Effective Implementation of Multiconformer Transition State Theory for Peroxy Radical Hydrogen Shift Reactions. *J. Phys. Chem. A* **2016**, *120*, 10072–10087.

[2] Vereecken, L.; Peeters, J. The 1,5-H-shift in 1-Butoxy: A Case Study in the Rigorous Implementation of Transition State Theory for a Multirotamer System. *J. Chem. Phys.* **2003**, *119*, 5159–5170.

[3] Chai, J.-D.; Head-Gordon, M. Long-range Corrected Hybrid Density Functionals with Damped Atom-atom Dispersion Corrections. *Phys. Chem. Chem. Phys.* **2008**, *10*, 6615–6620.

[4] Dunning, T. H. Gaussian Basis Sets for Use in Correlated Molecular Calculations. I. The Atoms Boron Through Neon and Hydrogen. *J. Chem. Phys.* **1989**, *90*, 1007–1023.

[5] Kendall, R. A.; Dunning, T. H.; Harrison, R. J. Electron Affinities of the First-row Atoms Revisited. Systematic Basis Sets and Wave Functions. *J. Chem. Phys.* **1992**, *96*, 6796–6806.

[6] Frisch, M. J.; Trucks, G. W.; Schlegel, H. B.; Scuseria, G. E.; Robb, M. A.; Cheeseman, J. R.; Scalmani, G.; Barone, V.; Mennucci, B.; Petersson, G. A. et al. Gaussian 09 Revision D.01. Gaussian Inc. Wallingford CT 2009.

[7] Werner, H.-J.; Knowles, P. J.; Knizia, G.; Manby, F. R.; Schütz, M.; Celani, P.; Györffy, W.; Kats, D.; Korona, T.; Lindh, R. et al. MOLPRO, Version 2012.1, a Package of Ab Initio Programs. 2012; see http://www.molpro.net.

[8] Watts, J. D.; Gauss, J.; Bartlett, R. J. Coupled-cluster Methods with Noniterative Triple Excitations for Restricted Open-shell Hartree-Fock and Other General Single Determinant Reference Functions. Energies and Analytical Gradients. *J. Chem. Phys.* **1993**, *98*, 8718–8733.

[9] Adler, T. B.; Knizia, G.; Werner, H.-J. A Simple and Efficient CCSD(T)-F12 Approximation. *J. Chem. Phys.* **2007**, *127*, 221106.

[10] Knizia, G.; Adler, T. B.; Werner, H.-J. Simplified CCSD(T)-F12 Methods: Theory and Benchmarks. *J. Chem. Phys.* **2009**, *130*, 054104.

[11] Werner, H.-J.; Knizia, G.; Manby, F. R. Explicitly Correlated Coupled Cluster Methods with Pair-Specific Geminals. *Mol. Phys.* **2011**, *109*, 407–417.

[12] Peterson, K. A.; Adler, T. B.; Werner, H.-J. Systematically Convergent Basis Sets for Explicitly Correlated Wavefunctions: The Atoms H, He, B–Ne, and Al–Ar. *J. Chem. Phys.* **2008**, *128*, 084102.

[13] Møller, K. H.; Bates, K. H.; Kjaergaard, H. G. The Importance of Peroxy Radical Hydrogen-Shift Reactions in Atmospheric Isoprene Oxidation. *J. Phys. Chem. A* **2019**, *123*, 920–932.

[14] Halgren, T. A. Merck Molecular Force Field. I. Basis, Form, Scope, Parameterization, and Performance of MMFF94. *J. Comput. Chem.* **1996**, *17*, 490–519.

[15] Spartan '14. Wavefunction Inc., Irvine, CA.

[16] Becke, A. D. Density-Functional Thermochemistry. III. The Role of Exact Exchange. *J. Chem. Phys.* **1993**, *98*, 5648–5652.

[17] Lee, C.; Yang, W.; Parr, R. G. Development of the Colle-Salvetti Correlation-Energy Formula into a Functional of the Electron Density. *Phys. Rev. B* **1988**, *37*, 785–789.

[18] Hehre, W. J.; Ditchfield, R.; Pople, J. A. Self—Consistent Molecular Orbital Methods. XII. Further Extensions of Gaussian—Type Basis Sets for Use in Molecular Orbital Studies of Organic Molecules. *J. Chem. Phys.* **1972**, *56*, 2257–2261.

[19] Clark, T.; Chandrasekhar, J.; Spitznagel, G. W.; Schleyer, P. V. R. Efficient Diffuse Function-augmented Basis Sets for Anion Calculations. III. The 3-21+G Basis Set for First-row Elements, Li–F. *J. Comput. Chem.* **1983**, *4*, 294–301.

[20] Frisch, M. J.; Pople, J. A.; Binkley, J. S. Self-consistent Molecular Orbital Methods 25. Supplementary Functions for Gaussian Basis Sets. *J. Chem. Phys.* **1984**, *80*, 3265–3269.

[21] Eckart, C. The Penetration of a Potential Barrier by Electrons. *Phys. Rev.* **1930**, *35*, 1303–1309.

[22] Clark, M.; Cramer, R. D.; Van Opdenbosch, N. Validation of the General Purpose Tripos 5.2 Force Field. *J. Comput. Chem.* **1989**, *10*, 982–1012.

[23] Tuazon, E. C.; Atkinson, R. A Product Study of the Gas-Phase Reaction of Isoprene with the OH Radical in the Presence of NO_x. *Int. J. Chem. Kinet.* **1990**, *22*, 1221–1236.

[24] Tuazon, E. C.; Alvarado, A.; Aschmann, S. M.; Atkinson, R.; Arey, J. Products of the Gas-Phase Reactions of 1,3-Butadiene with OH and NO_3 Radicals. *Environ. Sci. Technol.* **1999**, *33*, 3586–3595.

[25] Liu, X.; Jeffries, H. E.; Sexton, K. G. Hydroxyl Radical and Ozone Initiated Photochemical Reactions of 1,3-Butadiene. *Atmos. Environ.* **1999**, *33*, 3005 – 3022.

[26] Otkjær, R. V.; Jakobsen, H. H.; Tram, C. M.; Kjaergaard, H. G. Calculated Hydrogen Shift Rate Constants in Substituted Alkyl Peroxy Radicals. *J. Phys. Chem. A* **2018**, *122*, 8665–8673.

[27] Peeters, J.; Müller, J.-F.; Stavrakou, T.; Nguyen, V. S. Hydroxyl Radical Recycling in Isoprene Oxidation Driven by Hydrogen Bonding and Hydrogen Tunneling: The Upgraded LIM1 Mechanism. *J. Phys. Chem. A* **2014**, *118*, 8625–8643.

[28] Wennberg, P. O.; Bates, K. H.; Crounse, J. D.; Dodson, L. G.; McVay, R. C.; Mertens, L. A.; Nguyen, T. B.; Praske, E.; Schwantes, R. H.; Smarte, M. D. et al. Gas-Phase Reactions of Isoprene and Its Major Oxidation Products. *Chem. Rev.* **2018**, *118*, 3337–3390.

[29] Praske, E.; Otkjær, R. V.; Crounse, J. D.; Hethcox, J. C.; Stoltz, B. M.; Kjaergaard, H. G.; Wennberg, P. O. Atmospheric Autoxidation is Increasingly Important in Urban and Suburban North America. *Proc. Natl. Acad. Sci. U.S.A.* **2018**, *115*, 64–69.

[30] Su, T.; Chesnavich, W. J. Parametrization of the Ion–Polar Molecule Collision Rate Constant by Trajectory Calculations. *J. Chem. Phys.* **1982**, *76*, 5183–5185.

[31] Garden, A. L.; Paulot, F.; Crounse, J. D.; Maxwell-Cameron, I. J.; Wennberg, P. O.; Kjaergaard, H. G. Calculation of Conformationally Weighted Dipole Moments useful in Ion–Molecule Collision Rate Estimates. *Chem. Phys. Lett.* **2009**, *474*, 45 – 50.

[32] Paulot, F.; Crounse, J. D.; Kjaergaard, H. G.; Kroll, J. H.; Seinfeld, J. H.; Wennberg, P. O. Isoprene Photooxidation: New Insights into the Production of Acids and Organic Nitrates. *Atmos. Chem. Phys.* **2009**, *9*, 1479–1501.

[33] Crounse, J. D.; Paulot, F.; Kjaergaard, H. G.; Wennberg, P. O. Peroxy Radical Isomerization in the Oxidation of Isoprene. *Phys. Chem. Chem. Phys.* **2011**, *13*, 13607–13613.

[34] Spartan '16. Wavefunction Inc., Irvine, CA.

[35] Xu, L.; Møller, K. H.; Crounse, J. D.; Otkjær, R. V.; Kjaergaard, H. G.; Wennberg, P. O. Unimolecular Reactions of Peroxy Radicals Formed in the Oxidation of α-Pinene and β-Pinene by Hydroxyl Radicals. *J. Phys. Chem. A* **2019**, *123*, 1661–1674.

[36] Noble, R. W.; Gibson, Q. H. The Reaction of Ferrous Horseradish Peroxidase with Hydrogen Peroxide. *J. Biol. Chem.* **1970**, *245*, 2409–2413.

[37] Crounse, J. D.; Knap, H. C.; Ørnsø, K. B.; Jørgensen, S.; Paulot, F.; Kjaergaard, H. G.; Wennberg, P. O. Atmospheric Fate of Methacrolein. 1. Peroxy

Radical Isomerization Following Addition of OH and O_2. *J. Phys. Chem. A* **2012**, *116*, 5756–5762.

[38] Praske, E.; Otkjær, R. V.; Crounse, J. D.; Hethcox, J. C.; Stoltz, B. M.; Kjaergaard, H. G.; Wennberg, P. O. Intramolecular Hydrogen Shift Chemistry of Hydroperoxy-Substituted Peroxy Radicals. *J. Phys. Chem. A* **2019**, *123*, 590–600.

[39] Sharpe, S. W.; Johnson, T. J.; Sams, R. L.; Chu, P. M.; Rhoderick, G. C.; Johnson, P. A. Gas-Phase Databases for Quantitative Infrared Spectroscopy. *Appl. Spectrosc.* **2004**, *58*, 1452–1461.

[40] Cox, R.; Derwent, R.; Kearsey, S.; Batt, L.; Patrick, K. Photolysis of Methyl Nitrite: Kinetics of the Reaction of the Methoxy Radical with O_2. *J. Photochem.* **1980**, *13*, 149 – 163.

[41] Taylor, W. D.; Allston, T. D.; Moscato, M. J.; Fazekas, G. B.; Kozlowski, R.; Takacs, G. A. Atmospheric Photodissociation Lifetimes for Nitromethane, Methyl Nitrite, and Methyl Nitrate. *Int. J. Chem. Kinet. 12*, 231–240.

[42] Crounse, J. D.; McKinney, K. A.; Kwan, A. J.; Wennberg, P. O. Measurement of Gas-Phase Hydroperoxides by Chemical Ionization Mass Spectrometry. *Anal. Chem.* **2006**, *78*, 6726–6732.

[43] Vasquez, K. T.; Allen, H. M.; Crounse, J. D.; Praske, E.; Xu, L.; Noelscher, A. C.; Wennberg, P. O. Low-Pressure Gas Chromatography with Chemical Ionization Mass Spectrometry for Quantification of Multifunctional Organic Compounds in the Atmosphere. *Atmospheric Meas. Tech.* **2018**, *11*, 6815–6832.

[44] O'Haver, T. Pragmatic Introduction to Signal Processing 2019: Applications in scientific measurement. 2019; https://terpconnect.umd.edu/ toh/spectrum/InteractivePeakFitter.htm.

[45] MATLAB R2016b. 2016; The MathWorks, Natick, MA, USA.

[46] Berndt, T.; Scholz, W.; Mentler, B.; Fischer, L.; Herrmann, H.; Kulmala, M.; Hansel, A. Accretion Product Formation from Self- and Cross-Reactions of RO_2 Radicals in the Atmosphere. *Angew. Chem. Int. Ed.* **2018**, *57*, 3820–3824.

[47] Atkinson, R.; Baulch, D. L.; Cox, R. A.; Crowley, J. N.; Hampson, R. F.; Hynes, R. G.; Jenkin, M. E.; Rossi, M. J.; Troe, J. Evaluated Kinetic and Photochemical Data for Atmospheric Chemistry: Volume I - Gas Phase Reactions of O_x, HO_x, NO_x and SO_x Species. *Atmos. Chem. Phys.* **2004**, *4*, 1461–1738.

[48] Wallington, T. J.; Japar, S. M. Reaction of CH_3O_2+HO_2 in Air at 295 K: A Product Study. *Chem. Phys. Lett.* **1990**, *167*, 513 – 518.

[49] Wallington, T. J.; Japar, S. M. FTIR Product Study of the Reaction of $C_2H_5O_2$+HO_2 in Air at 295 K. *Chem. Phys. Lett.* **1990**, *166*, 495 – 499.

[50] Spittler, M.; Barnes, I.; Becker, K.; Wallington, T. Product Study of the $C_2H_5O_2$+HO_2 Reaction in 760 Torr of Air at 284–312 K. *Chem. Phys. Lett.* **2000**, *321*, 57 – 61.

[51] Hasson, A. S.; Tyndall, G. S.; Orlando, J. J. A Product Yield Study of the Reaction of HO_2 Radicals with Ethyl Peroxy ($C_2H_5O_2$), Acetyl Peroxy ($CH_3C(O)O_2$), and Acetonyl Peroxy ($CH_3C(O)CH_2O_2$) Radicals. *J. Phys. Chem. A* **2004**, *108*, 5979–5989.

[52] Teng, A. P.; Crounse, J. D.; Lee, L.; St. Clair, J. M.; Cohen, R. C.; Wennberg, P. O. Hydroxy Nitrate Production in the OH-Initiated Oxidation of Alkenes. *Atmos. Chem. Phys.* **2015**, *15*, 4297–4316.

[53] Miller, A. M.; Yeung, L. Y.; Kiep, A. C.; Elrod, M. J. Overall Rate Constant Measurements of the Reactions of Alkene-Derived Hydroxyalkylperoxy Radicals with Nitric Oxide. *Phys. Chem. Chem. Phys.* **2004**, *6*, 3402–3407.

[54] IUPAC Task Group on Atmospheric Chemical Kinetic Data Evaluation, h.-e. IUPAC Task Group on Atmospheric Chemical Kinetic Data Evaluation - Data Sheet HOx_VOC80.

[55] Howard, J. A. In *Peroxyl Radicals*; Alfassi, Z. B., Ed.; Wiley, New York, 1997; pp 283–334.

[56] Magneron, I.; Thévenet, R.; Mellouki, A.; Le Bras, G.; Moortgat, G. K.; Wirtz, K. A Study of the Photolysis and OH-initiated Oxidation of Acrolein and *trans*-Crotonaldehyde. *J. Phys. Chem. A* **2002**, *106*, 2526–2537.

[57] Kerr, J. A.; Sheppard, D. W. Kinetics of the Reactions of Hydroxyl Radicals with Aldehydes Studied under Atmospheric Conditions. *Environ. Sci. Technol.* **1981**, *15*, 960–963.

[58] Atkinson, R.; Aschmann, S. M.; Pitts, J. N. Kinetics of the Gas-Phase Reactions of OH Radicals with a Series of α,β-Unsaturated Carbonyls at 299 $\pm$ 2 K. *Int. J. Chem. Kinet.* **1983**, *15*, 75–81.

[59] Atkinson, R. Kinetics and Mechanisms of the Gas-Phase Reactions of the Hydroxyl Radical with Organic Compounds under Atmospheric Conditions. *Chem. Rev.* **1986**, *86*, 69–201.

[60] Orlando, J. J.; Tyndall, G. S. Mechanisms for the Reactions of OH with Two Unsaturated Aldehydes: Crotonaldehyde and Acrolein. *J. Phys. Chem. A* **2002**, *106*, 12252–12259.

[61] Orlando, J. J.; Tyndall, G. S. Laboratory Studies of Organic Peroxy Radical Chemistry: An Overview with Emphasis on Recent Issues of Atmospheric Significance. *Chem. Soc. Rev.* **2012**, *41*, 6294–6317.

[62] Atkinson, R.; Baulch, D. L.; Cox, R. A.; Crowley, J. N.; Hampson, R. F.; Hynes, R. G.; Jenkin, M. E.; Rossi, M. J.; Troe, J.; Subcommittee, I. Evaluated Kinetic and Photochemical Data for Atmospheric Chemistry: Volume II - Gas Phase Reactions of Organic Species. *Atmos. Chem. Phys.* **2006**, *6*, 3625–4055.

[63] Clayden, J.; Greeves, N.; Warren, S. *Organic Chemistry*; OUP Oxford, 2012.

[64] Jenkin, M. E.; Valorso, R.; Aumont, B.; Rickard, A. R.; Wallington, T. J. Estimation of Rate Coefficients and Branching Ratios for Gas-Phase Reactions of OH with Aliphatic Organic Compounds for use in Automated Mechanism Construction. *Atmos. Chem. Phys.* **2018**, *18*, 9297–9328.

[65] Jenkin, M. E.; Saunders, S. M.; Pilling, M. J. The Tropospheric Degradation of Volatile Organic Compounds: a Protocol for Mechanism Development. *Atmos. Environ.* **1997**, *31*, 81 – 104.

[66] Atkinson, R. Kinetics and Mechanisms of the Gas-Phase Reactions of the NO_3 Radical with Organic Compounds. *J. Phys. Chem. Ref. Data* **1991**, *20*, 459–507.

[67] Cabañas, B.; Salgado, S.; Martín, P.; Baeza, M. T.; Martínez, E. Night-time Atmospheric Loss Process for Unsaturated Aldehydes: Reaction with NO_3 Radicals. *J. Phys. Chem. A* **2001**, *105*, 4440–4445.

[68] Symons, M. C. R. Shape of Alkyl Radicals by Electron Spin Resonance. *Nature* **1969**, *222*, 1123–1124.

[69] Orlando, J. J.; Tyndall, G. S.; Paulson, S. E. Mechanism of the OH-Initiated Oxidation of Methacrolein. *Geophys. Res. Lett.* **1999**, *26*, 2191–2194.

[70] Tuazon, E. C.; Atkinson, R. A Product Study of the Gas-Phase Reaction of Methyl Vinyl Ketone with the OH Radical in the Presence of NOx. *International Journal of Chemical Kinetics* **1989**, *21*, 1141–1152.

[71] Galloway, M. M.; Huisman, A. J.; Yee, L. D.; Chan, A. W. H.; Loza, C. L.; Seinfeld, J. H.; Keutsch, F. N. Yields of Oxidized Volatile Organic Compounds During the OH Radical Initiated Oxidation of Isoprene, Methyl Vinyl Ketone, and Methacrolein under High-NOx Conditions. *Atmos. Chem. Phys.* **2011**, *11*, 10779.

[72] Praske, E.; Crounse, J. D.; Bates, K. H.; Kurtén, T.; Kjaergaard, H. G.; Wennberg, P. O. Atmospheric Fate of Methyl Vinyl Ketone: Peroxy Radical Reactions with NO and HO_2. *J. Phys. Chem. A* **2015**, *119*, 4562–4572.

[73] Atkinson, R.; Baulch, D. L.; Cox, R. A.; Hampson, R. F.; Kerr, J. A.; Rossi, M. J.; Troe, J. Evaluated Kinetic, Photochemical and Heterogeneous Data for Atmospheric Chemistry: Supplement V. IUPAC Subcommittee on Gas Kinetic Data Evaluation for Atmospheric Chemistry. *J. Phys. Chem. Ref. Data* **1997**, *26*, 521–1011.